19960607 156

MECHANICS OF LOAD TRANSFER AT THE FIBER/MATRIX INTERFACE

by Christos C. Chamis

Lewis Research Center

Cleveland, Ohio 44135

1. Report No. NASA TN D-6588	2. Government Accession No.	3. Recipient's Catalog No.
4. Title and Subtitle MECHANICS OF LOAD TRANSFER AT THE FIBER/MATRIX INTERFACE		5. Report Date February 1972
		6. Performing Organization Code
7. Author(s) Christos C. Chamis		8. Performing Organization Report No. E-6447
		10. Work Unit No. 134-14
9. Performing Organization Name and Address Lewis Research Center National Aeronautics and Space Administration Cleveland, Ohio 44135		11. Contract or Grant No.
		13. Type of Report and Period Covered Technical Note
12. Sponsoring Agency Name and Address National Aeronautics and Space Administration Washington, D.C. 20546		14. Sponsoring Agency Code

15. Supplementary Notes

16. Abstract

The role of the fiber/matrix interface on composite structural integrity and strength is discussed. The major part of the information contained herein is drawn from the published literature. Some recent results obtained by the author and his associates are included to project some current thinking. Methods for measuring and predicting interface bond stresses and interface bond strength are described. Geometric and material variables which influence interface stress and interface bond strength are identified. The dependence of composite fracture surface characteristics on bond strength is illustrated. Parameters for selecting constituents to yield specified interface bond strength are recommended.

17. Key Words (Suggested by Author(s)) Fiber composites; Interface; Interface stress state; Interface bond strength; Composite structural integrity; Composite strength; Experimental stress analysis; Theoretical stress analysis; Finite element; Review	18. Distribution Statement Unclassified - unlimited

19. Security Classif. (of this report) Unclassified	20. Security Classif. (of this page) Unclassified	21. No. of Pages 64	22. Price* $3.00

MECHANICS OF LOAD TRANSFER AT THE FIBER/MATRIX INTERFACE

by Christos C. Chamis

Lewis Research Center

SUMMARY

The literature is reviewed to assess the role of the fiber/matrix interface on composite structural integrity. Recent results obtained by the author are included to indicate some current trends.

Various theoretical and experimental methods which have been developed to assess the interface bonding condition are summarized. Results obtained using these methods are presented to illustrate their applicability and limitations. Geometric and material variables which influence the stress and bond strength at the interface are identified. Their effects on composite structural integrity and strength are illustrated. The relation of composite fracture surface characteristics to bond strength is also illustrated.

The results examined and summarized lead to the following conclusions: The better the interface bond, the higher is the static composite strength. High interface bond strength results in brittle and notch-sensitive composites. Typical tests for interface bond strength include matrix Poisson effect, fiber pullout, fiber pushthrough, short-beam-horizontal shear, transverse tensile, dynamic modulus, and photoelasticity. Analysis methods include mechanics of materials, classical elasticity, and finite element. Microresidual stresses and longitudinal loads along the fiber direction set up forces which tend to break the bond. The presence of voids at the interface weakens the bond. Elevated-temperature environments degrade the interface bond. When a fiber breaks within the composite, the energy released tends to debond the interface. The matrix effects on the bond are indicated by a debonding parameter. This debonding parameter can be used to design the interface bond for specific composite applications.

INTRODUCTION

It is well known in the fiber composite technology community that the fiber/matrix interface gives fiber composites their structural integrity. The interface consists of the bond between fiber and matrix and the immediate region adjacent to this bond (fig. 1). The interface is usually considered to be of zero thickness for analysis purposes. At

least three types of bonding are thought to exist at the interface. These are chemical, electrical, and mechanical. Irrespective of the nature of the bond, the load transfer is primarily a mechanistic process.

The role of the interface on composite structural integrity is better appreciated when it is realized that 1 cubic inch of 50-volume-percent fiber composite with a fiber diameter of 0.0003 inch contains approximately 6500 square inches of interface area. The fiber/matrix interface has been extensively investigated in references 1 to 3. The reviews in references 4 to 9 are excellent sources for obtaining a good assessment of some specific aspects of the problem.

From the load-transfer mechanics viewpoint, experimental and theoretical stress analysis dealing with the stress state at the interface are of special interest. Experimental works on the stress state at the interface are reported in references 10 to 15 for model studies and in references 16 to 18 for multifiber inclusions. Theoretical studies on the stress state at the interface are summarized in references 19 to 23 for axial load transfer and in references 24 and 25 for transverse and shear load transfer using simplified models. Theoretical studies for axial load transfer based on classical elasticity are reported in references 26 to 29. Corresponding studies for transverse load transfer are reported in references 30 to 34. The finite element method of analysis has also been employed to investigate the stress state at the interface (refs. 35 to 39). Additional pertinent references are mentioned in reference 40.

There are, in general, five idealization assumptions underlying all the theoretical studies. They are (1) elastic constituent material behavior, (2) zero thickness for the interface, (3) perfect bond, (4) identical constituent bulk and in-situ properties, and (5) a regular or repeating array of fibers. It is known that actual composites violate most, if not all, of the aforementioned assumptions. However, the theoretical predictions still are an invaluable tool in identifying important local geometry and material variables and in obtaining quantitative estimates of the stress state at the interface.

The objective of this report is to discuss the mechanism of load transfer from matrix to fiber through the interface and, as a consequence, the effects of the interface on composite structural integrity. Specifically the report deals with the role of interfacial bond in composite strength, the dependence of fracture surface on the interface bond strength, methods for measuring and predicting the stress at the interface, the microresidual stress and load condition effects on the interface bond, and the effects of voids and fiber breaks on the interface bond. Also the possibility for designing composites with specified bond properties is examined. Many of these effects are illustrated graphically to indicate general trends and to illustrate significant points.

The discussion is based on theoretical considerations and is supplemented with pertinent experimental data. The major part of the information is drawn from the published literature. In this respect the report serves as a state-of-the-art report. Recent

2

results obtained by the author and his associates at NASA Lewis are included to project some current trends and thinking. Since the field is still in a highly fluid state, definitive conclusions and overgeneralizations could be misleading at this time. However, certain important aspects are emphasized whenever possible.

INTERFACE BOND: TYPICAL EXAMPLES AND MECHANISTIC MODELS
FOR LOAD TRANSFER

The interface in a fiber/matrix composite is a surface which is common to both fiber and matrix and the immediate region about this surface. It has physical and mechanical properties which are neither those of the fiber nor those of the matrix.

An interesting example of fiber/matrix interface is illustrated in figure 1 which shows scanning electron photomicrographs of graphite fibers in a resin matrix. The fiber is shown rather clearly, and the matrix is also shown. In this particular case, the interface is the region which is next to the fiber surface and adjacent to the matrix surrounding the fibers.

The failure or damage of the interface near the fiber region is illustrated in figure 2. In this figure, the crack seems to have initiated at that point where the fibers are the closest. As can be seen, the crack followed a path along the circumference of the fibers.

Additional illustrations of crack initiation or failure of the interface bond are presented in figure 3. In figure 3(a), a single fiber embedded in a matrix casting is shown. The composite was subsequently pulled in the direction normal to the fiber. The Poisson effect in the matrix induces high shear stress at the ends of the fibers, forcing the bond to break. The result can be seen at the left end of the fiber in figure 3(a). In figure 3(b) the fractured surface of such a model study is shown. As can be seen, the matrix has fractured in a cleavage mode, while the fiber has remained intact.

A mechanistic representation of how the load is transferred from the matrix to the fiber in a short-fiber composite is illustrated in figure 4. In figure 4(a) the deformation pattern is shown. In figure 4(b) the shear and axial stress distributions are shown for elastic load transfer. In figure 4(c) the shear and axial stress distributions are shown for the elastic-plastic and inelastic cases. There are three points of interest to be noted in figures 4(b) and (c):

(1) The shear stress at the interface increases rapidly to a peak value and then decays rapidly away from the fiber end.

(2) The axial stress in the fiber increases rapidly to its average value, the value the fiber attains in the composite, and remains constant at this value for the elastic case.

(3) For the elastic-plastic case, the shear stress at the interface increases to a value that will cause the interface or matrix to behave inelastically (plastically). The

3

shear stress will stay at this value for some distance along the fiber until the greater portion of the load has been transferred to the fiber and then it will decay rapidly.

An additional mechanistic model of load transfer is illustrated in figure 5. All the essentials of the load-transfer mechanisms are illustrated. These physical concepts are fundamental in constructing theories for predicting the load transfer through the interface. Figure 5(b) is noteworthy in that the shear goes in one direction from one end of the fiber, whereas it reverses direction at the other end. Also, the shear stress reaches a maximum value near the end of the fiber. It decreases rapidly to zero along the fiber length where the normal stress in the fiber has achieved its composite average value. Near the other end of the fiber the interface shear stress increases gradually at first, rapidly reaching its peak value at the end of the fiber.

ROLE OF INTERFACE BOND ON COMPOSITE STRUCTURAL INTEGRITY

The role that the interface plays in the structural integrity of the composite and subsequently in its strength is described in this section. The effect that the interface has on the elastic constants of the composite and on the matrix strain magnification and how these factors affect the structural integrity of a composite are described. In particular, theoretical and experimental results are compared, where the theoretical results account for some aspect of the bonding condition at the interface.

A brief description of how fiber/resin composites are fabricated, in general, will be helpful in understanding the subsequent discussion. The tape from which a unidirectional composite, lamina, or ply is made is fabricated in the following manner. Single or multifiber ends from several spools are arranged in tape form and are taken through a matrix bath. The resin-impregnated tape is wound on a mandrel and partially cured, or B-staged. This B-staged material, called prepreg tape, is used to make composites of specified ply orientation, stacking sequence, and thickness.

An end, yarn, or bundle of fibers going into a ply is schematically illustrated in figure 6. It can be seen that the end of fibers goes into a square of dimensions t_l by t_l, or into a rectangle of dimensions t_l by some constant times t_l. The rectangle is probably more representative of the physical situation. From this rectangle, a repeating or typical subelement is selected as is indicated in the sketch entitled "repeating element for square array." Here the essential dimensions and terms commonly used in micromechanics are identified.

The repeating element of figure 6 is a typical model used in micromechanics theories for composite strength, thermal, and other mechanical behaviors. Using this model and assuming perfect bond at the interface, one can, by using the simple rule of mixtures, derive expressions for predicting the longitudinal modulus of the composite

4

(the modulus along the fiber direction) and the corresponding Poisson's ratio. Such theoretical predictions are compared with experimental data in figure 7 for an E-glass epoxy composite. As can readily be seen in this figure, the agreement between theory and experiment is rather good. The point to be made from this comparison is that the assumption of perfect bond along the interface is reasonable since both experiment and theory are in good agreement. Or possibly the variables plotted in figure 7 are insensitive to interfacial bonding imperfections.

Corresponding results based on a square array for the transverse modulus are illustrated in figure 8. In this figure, the transverse modulus is plotted as a function of fiber volume ratio for three different void contents. Theoretical as well as experimental data are shown in this figure. Unfortunately, the actual void content in these composites was not measured. An important point to be made from this figure is that the transverse modulus is an indirect but sensitive measure of the quality of the bond at the interface.

Simplified models used in predicting strength by micromechanics are illustrated in figure 9. In this figure, two elements are identified. One is the element for transverse strength, and the other is the element for intralaminar shear strength.

The model for the transverse strength leads to an equation which predicts the average strain the matrix as a function of the average transverse strain in the composite. This strain can be compared directly with the allowable matrix strain or it can be converted to a stress using the stress-strain diagram of the matrix. Analogous considerations lead to similar conclusions for the shear model. This type of model and analysis is called the strain magnification method. It is used to compute the transverse and intralaminar shear strengths of the ply (refs. 24 and 25).

Using the previously described models, the transverse strain magnification factor is shown as a function of fiber volume ratio for three composite systems in figure 10. In this figure the transverse ply modulus is also shown. There are two important points to be made in connection with figure 10: (1) as the fiber content increases, both the transverse ply modulus and the strain magnification factor increase; (2) the strain magnification factor for the boron composite increases at a greater rate than either the corresponding strain magnification factors or moduli of the other two fiber/matrix systems. The analytical results presented in figure 10 were obtained on the basis of a perfect bond. Later (p. 15), results are presented where imperfect bond and voids in the matrix or interface are taken into account. Their effects on composite transverse and intralaminar shear strengths are illustrated.

DEPENDENCE OF FRACTURE SURFACE MORPHOLOGY
ON INTERFACE BOND STRENGTH

The type of fracture surface is a good indicator of the type of bond at the interface. A strong bond, an intermediate bond, or a weak bond each results in a fracture surface which is distinctly different. These types of surfaces are examined in this section.

Typical fracture surfaces of unidirectional composites loaded in tension along the fiber direction are schematically illustrated in figure 11. The fracture surface of a specimen with a strong bond is shown in figure 11(a). The fracture surface is fairly smooth across the cross section. Composites exhibiting this type of fracture surface are known to have high static strength and tend to be notch sensitive. In figure 11(b) the fracture surface of a specimen with intermediate bond strength is illustrated. This fracture surface is irregular and has some fiber pullout. In figure 11(c) the fractured surface of the composite with very poor interface bond is illustrated. This type of specimen exhibits pronounced irregularity and fiber pullout. Reference 41 provides a more detailed description, including actual photographs of fractured tensile specimens, of the dependence of the fracture surface on the quality of the interfacial bond.

Photomicrographs of fractured specimens are shown in figure 12. The fracture surface of a unidirectional composite with intermediate bond strength is shown in figure 12(a). Note the considerable amount of fiber pullout and the irregular fracture surface. In figure 12(b) the transverse fracture surface for the same composite is shown. Here the fracture is much more brittle and the fracture surface traverses matrix as well as fibers and interface. The fracture surface of a composite which has better bond strength is shown in figure 12(c), where a much smaller amount of fiber pullout is evident. The corresponding transverse fracture surface is shown in figure 12(d). Here again, the fracture is quite brittle and restricted to one plane.

The fracture surface of a multilayered composite is illustrated in figure 13. This composite is made of plies oriented $\pm 45^{\circ}$ with Thornel-50S fibers. The type of load and direction and the photograph view angle are shown in the sketch in the figure. The fracture surface of this composite exhibits both longitudinal type (figs. 12(a) and (c)) the transverse type (figs. 12(b) and (d)) fracture characteristics.

These examples clearly illustrate that the type of bond quality at the interface plays a predominant role as to the type of fracture surface that a composite will exhibit when it is loaded in the fiber direction. When the composite is loaded in the transverse direction, the fracture surface is predominantly brittle and traverses matrix and interface as well as some fibers.

METHODS FOR MEASURING INTERFACE BOND STRENGTH

There are several methods which can be used to obtain a measure of the stress state and the strength of the bond at the interface. These methods can be divided into two groups. One group deals with direct measurements and could involve either model studies with single fibers in a matrix casting or multifibers. The other group involves indirect measure of the bond strength at the interface. The second group can also be viewed as a qualitative test; however, when interpreted properly, it could serve as a quantitative test. Both methods are described subsequently.

The most common test and perhaps the easiest to use in measuring bond strength is the fiber pullout strength test, also known as the button test, illustrated in figure 14. In figure 14(a) a schematical arrangement of the test setup is given, where the essential parts are clearly identified. In figure 14(b) the plot that is made in connection with this test is shown. The test results identified as tensile failure denote fiber breaks, and shear failures denote fiber pulled out from the matrix. Straight lines drawn through the points of shear failures and tensile failures intersect at a point in this plot. This point defines what is known in the field as the critical length. It is seen from figure 14(b) that the critical length is that fiber length which is required for the fiber to develop its full strength in the matrix. It is worth noting that this length is very, very small, being a little more than three fiber diameters for the system illustrated in figure 14(b). Additional results at elevated temperatures are given in figure 14(c). In figure 14(c) the critical length is easily identified; it is apparent that it depends on the temperature, as well as on the constituent materials.

Another method to establish the bond strength at the interface is presented in figure 15, where the force required to push a disk of the matrix along the fiber is plotted as a function of the crosshead movement. There are two interesting points to be observed in figure 15:

(1) The force against crosshead movement reaches a peak which is identified as bond peak in this figure. This indicates that this peak is the bond strength of the interface.

(2) Subsequent force to drive the disk along the fiber is associated with the friction force as a result of the residual stress which exists at the interface. This stress resulted from the thermal expansion mismatch of the constituents.

The mechanisms illustrated in figure 15 demonstrate that the interface has at least two modes of transferring load from the matrix to the fiber: the first being the bond that exists at the interface, and the second being the friction force. How much each of these contributes or to what extent the friction force assists in transferring load through the interface still remains a controversial subject. Additional experimental modes which demonstrate the effect of the friction force on the load transfer are discussed in reference 42.

Direct measurements using models illustrated in figure 16(a) are used to obtain the shear strength and the tensile strength at the interface. The model for the bond shear strength at the end of the fiber is the one which has a constant cross section, while the model for the tensile strength is the neck-down specimen. Corresponding results from these models are given in figure 16(b) for tensile strength and in figure 16(c) for the shear strength. From figure 16(b) the tensile strength for a boron fiber in an epoxy is approximately 800 psi. The shear strength from figure 16(c) is seen to be approximately 8000 psi. It is apparent that the shear strength at the interface is much greater than the tensile strength. The effects of various treatments on the fibers are also shown in this figure. The treatment has little or no effect on the tensile bond strength, whereas it has a considerable effect on the shear bond strength.

Indirect methods to measure the interface bond strength include the intralaminar shear strength test and the transverse strength test. Results obtained using the intralaminar shear strength test are illustrated in figure 17. In figure 17(a) short-beam shear strengths are plotted as a function of deflection for various graphite/fiber composites. The fibers associated with these composites are identified in the table in figure 17. The point to be noted from these results is that the fiber microstructure, as reflected by its modulus and the type of fiber surface treatment, affects intralaminar shear strength and, therefore, influences the interfacial bond. An indication of the intralaminar shear strength dependence on fiber modulus is illustrated in figure 17(b) for composites with untreated fibers.

Stress distribution results from transverse loading, as measured by photoelastic studies, are given in figure 18. The load direction and the essential variables of this test method are noted in the sketch. Nondimensional plots for the three normal stresses in the matrix at points on a line between fibers are plotted for a composite system of approximately 50-percent fiber volume ratio. The normalizing parameter is the applied stress. Three points of interest are as follows:

(1) The radial stress, or the stress which tends to enhance or weaken the available bond strength, is maximum at the point midway between the fibers and minimum at the interface.

(2) The hoop stress, which tends to crack or craze the matrix around the fiber, is minimum at the point midway between fibers and maximum at the interface.

(3) All the stresses have approximately equal magnitudes at the interface, indicating a condition of hydrostatic stress at this point in the interface.

Results of transverse strength tests of the composite as an indirect measure of the bond strength are illustrated in figure 19(a). Longitudinal tensile strengths are also shown for comparison purposes in figure 19(b). The strengths are plotted as a function of fiber volume ratio. The longitudinal tensile strength reaches a peak at approximately 60-volume-percent fiber and then it decreases. It can be seen in figure 19(a) that the

transverse strength decreases as the fiber content increases. The results in this figure indicate that the transverse tensile strength is a sensitive test for assessing the interfacial bonding condition. A properly designed flex test with fibers parallel to the beam's longitudinal axis is another sensitive indirect test method for assessing the quality of interfacial bond (ref. 43).

The dynamic modulus as well as the log decrement have also been used to obtain a measure of interfacial bond condition. Results for dynamic shear modulus and the corresponding log decrement are illustrated in figure 20 for a particulate composite. In figure 20(a) dynamic shear moduli for reinforced and unreinforced matrix systems are given as a function of axial strain of the composite. In figure 20(b) results for the log decrement are presented. As can be seen in these figures, both the reinforcement and the axial strain affect the dynamic response of this composite. Also the high axial strain rate damages the bonding condition at the interface as measured by the dynamic shear modulus or the log decrement.

A model for measuring the shear fracture energy at the interface is reported in references 13, 44, and 45 and is illustrated in figure 21. In this figure both a schematic and polarized light picture are shown. The fracture energy has also been used to measure bond strength with the aid of the double-cantilevered cleavage specimen illustrated in figure 22(a). The energy measured for a particulate composite is shown in figure 22(b), where it can be seen that the treatment affects the fracture energy. The point to be noted in figure 22(c) is that, once the crack starts propagating, the load remains nearly constant until the crack propagates the length of the cantilever. Other methods of nondestructive evaluation have also been used with some success to assess the interface bond (refs. 46 to 48).

METHODS FOR PREDICTING THE STRESS AT THE INTERFACE

Several methods have been proposed for predicting the stress state at the interface, which can then be used to estimate the bond strength. The shear lag method has received extensive treatment (refs. 19 and 20). This method is primarily used to determine the interface shear stress concentration at the end of the fiber as well as shear stress variation along the fiber. Additional methods include the Lame' solution for a shrink fit, classical elasticity boundary-value problems, and finite element analysis.

A schematic of the model on which various analytical methods are based is illustrated in figure 23. A longitudinal section of the composite having a hexagonal fiber array is shown and all the pertinent elements are identified.

Shear stress distribution factors at the interface predicted by various investigators for a single fiber embedded in a matrix are compared in figure 24. The normalized

shear stress distribution is plotted as a function of the number of fiber diameters from the end of the fiber. The maximum stress concentration is at the end of the fiber and has values ranging from approximately 2.5 to almost 4. Though the boundary conditions used to obtain the results in figure 24 are not described here in detail, suffice it to say that the maximum stress concentration at the end of the fiber depends very much on the boundary conditions selected.

Interface shear stress concentration factors at the end of a broken fiber in a composite as predicted by shear-lag theory using the model in figure 23 are shown in figure 25. To obtain these results it was assumed that the fiber had no load at its free end and achieved a maximum load equal to its average value in the composite at some distance from the end. The points to be noted from figure 25 are

(1) The maximum shear stress concentration at the end of a broken fiber in the composite is not as high as was indicated in figure 24 for the single fibers.

(2) The maximum shear stress concentration depends on the fiber type as well as on the fiber volume ratio.

The values of shear stress concentration, here, range from about 0.1 to 0.3 in the range of practical fiber volume ratios. These values seem to be realistic when one thinks of the actual tensile load or stress of the composite along the fiber direction. The following example illustrates this point. Consider a boron composite with 50-volume-percent fiber loaded to 100 000 psi, which is about 50 percent of its ultimate strength. The corresponding maximum shear concentration at the free end of a fiber, according to the results of figure 25, will be about 10 000 psi. Usage of figure 24 for this example will be inappropriate and the result will be erroneous and totally misleading. Two additional points to be noted from figure 25 are

(1) The maximum shear stress concentration at the end of the fiber remains almost invariant at intermediate fiber volume ratios.

(2) It increases rather rapidly at low and high fiber volume ratios.

The finite element method of analysis has also been employed to investigate the stress state at the end of the fiber in single-embedded-fiber model studies. A typical model in a finite element analysis is illustrated in figure 26. The figure shows the physical problem examined and the resulting stress distributions at the end and along the fiber. The results obtained from this method of analysis are given in figure 27. In figure 27(a) the shear stress is plotted as a function of a fiber diameter distance, and in figure 27(b) the corresponding axial stress in the fiber is plotted. Analytical results from other methods are superimposed on these plots for comparative purposes. It can be seen that results obtained by using classical and finite element methods are in good agreement.

Finite element analysis results obtained using a single-fiber model system with various boundary conditions are reported in reference 35. Some of the results are repro-

duced here. In figures 28(a) and (b) the schematic of the models studied and the displacement distribution along the fiber are illustrated. In figure 28(c) the shear and axial stress distributions are given as a function of fiber length-to-diameter ratio. It is of interest to note in this plot that the fiber axial stress is not zero at the end but has some finite value. In this particular analysis, the investigators assumed that the fiber end was bonded to the matrix. This is further seen in figure 28(d) where the "end-bond-broken" and "end-bond-intact" curves are shown. The maximum shear stress along the fiber length as a function of fiber length-to-diameter ratio as well as the shear stress at the interface are plotted in figure 28(e). The maximum shear stress is constant after approximately two to three diameter distances from the fiber end. The reason for this is that components from both the interfacial shear stress and axial stress are combined, resulting in the near-constant value. This would suggest a possibility for designing the bond strength in such a way that this maximum shear stress value does not exceed some equivalent allowable matrix stress. One has to keep in mind that the use of the equivalent allowable stress concept is a carryover from homogeneous isotropic material failure theories and should be used with caution.

Additional results from the studies of reference 35 are illustrated in figure 29. The radial stress variation along the fiber length is shown in figure 29(a). The maximum matrix axial stress for different fiber end geometries (elliptic, circular, or tapered) is presented in figure 29(b), and the corresponding maximum shear stress in figure 29(c). It can be seen from these results that the maximum stress concentration at the end of the fiber is not only a function of the constituents but also a function of the type of fiber end geometry as well as whether or not the fiber end is bonded to the matrix. An interesting observation from figure 29(b) is that the minimum matrix axial stress concentration is obtained using hemispherical-end fibers.

Results from other theories are discussed in the following sections, where the microresidual stress and the longitudinal load effects on the interface are examined.

MICRORESIDUAL STRESS EFFECTS ON INTERFACE BOND STRENGTH

The fabrication process used to make fiber composites inherently produces microresidual stresses at the interface. Both experimental and analytical methods have been advanced to investigate the microresidual stress state at the interface and to obtain an estimate of its effects on available interfacial bond strength.

The results of a photoelastic investigation of a multifiber inclusion model are given in figure 30. The fiber arrangement for this investigation is the square array. The fiber volume ratio for the system investigated is approximately 0.5. On this plot, all three stresses are plotted as a function of a radial distance from a reference point which is

midway between fibers. The schematic illustrating the reference point is also shown in figure 30. The stresses are normalized with respect to the radial stress in a single inclusion, and its value is also given in the schematic. It is seen from the stress results in figure 30 that the microresidual stress in the radial direction is maximum at the interface and is compressive. Conversely, the hoop stress is tensile and is maximum at the point midway between the fibers, achieving a minimum value at the interface. The longitudinal stress is also tensile and remains almost constant between fibers. This is an important result because simplified micromechanics analyses for microresidual stress assume the longitudinal residual stress to be constant in the matrix. The value that the residual radial stress of a typical boron composite will reach at the interface is approximately 4500 psi. The corresponding hoop stress will have a value of approximately 2000 psi at interface and is tensile. As was already mentioned, tensile hoop stress tends to craze or crack the matrix around the fiber. For the system in figure 30, a value of 2000 psi is probably not large enough to cause any damage, assuming that no voids exist to aggravate the condition at the interface. Additional photoelastic studies are reported in reference 18. The results reported in reference 18 include the stress distribution along the fiber circumference for various fiber contents and different constituent materials.

Classical elasticity analytical results for microresidual stresses based on models of figures 23 and 31 are shown in figure 32. For this particular analysis it was assumed that the matrix shrank 1 percent and the fibers did not shrink at all. This would correspond to a fiber/epoxy composite with cure temperature differential of approximately 300° F. Typical results from this classical analysis are shown in figure 32. All the pertinent stresses are plotted as a function of the arc distance from the 0° to the 30° symmetry lines. This 30° segment is sufficient to completely describe the stress distribution around the fiber because a hexagonal array possesses a twelvefold symmetry (fig. 31). The results are also plotted as a function of the relative stiffness of the constituents. The points to be observed from these results are the following:

(1) The residual radial stress at the interface is compressive at the 0° symmetry line and its magnitude is a function of the relative stiffness of the constituents.

(2) The residual radial stress at the interface is a function of position along the circumference. It changes from compressive to tensile as it approaches the other symmetry line, which is 30° in this particular example.

(3) The axial stress is tensile as was the case for the experimental results (fig. 30).

(4) The hoop stress remains tensile everywhere.

(5) Shear stress varies along the fiber circumference, reaching a maximum value at about 10° to 15°.

In figure 33, corresponding results are shown where the stiffness of the constituents is constant and the fiber volume ratio is varied. These results indicate trends similar to

those in figure 32, with the addition that the maximum stress at the interface increases as the fiber content increases.

The three points to be kept in mind from the discussion of these analytical results of microresidual stress are

(1) The radial stress at the interface can be either tensile or compressive; its value depends on the stiffness of the constituents and increases as the E_f/E_m ratio decreases. It also depends on the fiber volume ratio and increases as this ratio increases.

(2) Shear stress exists along the fiber circumference and tends to locally rotate the fiber within the matrix.

(3) The hoop stress at the interface in the matrix or interfacial bond is tensile and of relatively high magnitude.

It should also be noted that the experimental results (fig. 30) indicate that the microresidual radial stress is maximum midway between the fibers, whereas the analytical results indicate that it is maximum at the interface. However, both analytical and experimental results agree that the hoop and axial residual stresses in the matrix are tensile.

Photoelastic investigations concerning the stress distribution in models with two fiber inclusions of different diameter are described in reference 14. Photoelastic studies on multifiber inclusions are described in references 17 and 18. Analytical results for residual stress, in addition to those discussed previously, are also given in references 30 and 49. The results of reference 49 for a Thornel-40/epoxy show that the residual radial stress is compressive around the fiber circumference for the square array model investigated.

LOADING CONDITION EFFECTS ON INTERFACE BOND

The interface bond is affected by the type of loading condition imposed on the composite. The effects of the transverse load have previously been discussed. In this section we discuss the longitudinal load effects. Analytical results dealing with this type of loading and based on the hexagonal fiber array arrangement are illustrated in figure 34. The results presented subsequently are for isotropic constituent materials and are for the arc from 0° to 30°. The stress distribution along this arc completely describes the stress state around the fiber because of symmetry as described in the previous section.

The stress distribution at the interface along the arc between 0° and 30° is given in figure 34 for longitudinal loading. In figure 34(a), the radial stress is plotted as a function of the angle for various relative stiffnesses of the constituents. As can be seen in this figure, the radial stress at the interface at the 0° line has the opposite sign of the

applied stress and it increases continuously, reaching a maximum stress of the same size as the applied stress at the 30° line. In figure 34(b) results are plotted for circumferential (in the r-θ plane) shear stress. It is important to note that circumferential shear stresses do exist along the fiber circumference at the interface when the composite is loaded longitudinally. These stresses are constant along the fiber length away from the ends. In contrast, the longitudinal shear stresses exist only near the fiber ends. Axial stress variation in the matrix along the interface is plotted in figure 34(c) and the corresponding stress in the fiber in figure 34(d). The points to be noted, from these results, are

(1) The stress at the interface increases as the constituent stiffness ratio E_f/E_m decreases.

(2) The matrix axial stress at the interface is maximum at the end of the fiber and decreases very rapidly.

(3) The maximum concentration factor for the matrix axial stress is 3 or greater, which again seems to be unreasonable for the physical conditions as was discussed previously.

Crossplots of the results in figure 34, where the constituent stiffnesses remain constant but the fiber volume ratio is varied, are presented in figure 35. The stresses illustrated here are the radial stress, the shear stress, and the hoop stress along the arc of the fiber from 0° to 30°. The point to be noted from these results is that the stresses at the interface as a function of the applied load increase with increasing fiber volume ratio.

It is possible to superimpose analytical results obtained for the microresidual stress due to external load. This was done in reference 5 for the stresses at the interface. The results are summarized in table I. The results shown in this table are self-explanatory. The important point to be noted is that the maximum combined radial tensile stress at the interface occurs at 30°. For the case investigated, the combined radial stress reaches a value of approximately 2300 psi. Direct measurement of the bond strength previously discussed showed it to be about 800 psi. Comparing these two values, it would seem that the 2300 psi has sufficient magnitude to break the interfacial bond at this particular point. The combined hoop stress at the 30° line reaches magnitudes of approximately 12 000 to 15 000 psi. This value is approximately of the same magnitude as that of the resin matrix tensile strength. It can be concluded then, that for the conditions examined here, the matrix around the fibers at the interface will craze or crack and thus damage the interfacial bond.

It should also be noted that the shear stress along the circumference reaches magnitudes which are comparable to those of the shear bond strength mentioned previously. The main point to be remembered from these results is that residual stresses and stresses from axial loads can result in stress states at the interface of substantial mag-

nitude which are comparable to either the tensile strength of the interface bond or the tensile strength of the matrix. Additional results are reported in references 26 and 27. In reference 27, the fiber is assumed to be orthotropic, whereas the results previously discussed were for isotropic fibers.

EFFECTS OF VOIDS AND ENVIRONMENT ON INTERFACE BOND STRENGTH

Experimental investigations have shown that voids are detrimental to composite integrity and to its strength. Environmental effects also have significant effects on the composite integrity and strength. Both voids and environmental effects will affect the interfacial bond. These effects are examined in this section.

The effect of voids on the interface, which is suggested by the transverse ply strength, is illustrated in figure 36. In figures 36(a) and (b) voids in the matrix and at the interface are illustrated by a schematic and a photomicrograph. In figure 36(c) the volume ratio of ineffective fibers, that is, fibers with voids at the interface which cannot transmit transverse load, is plotted against the void volume ratio. The transverse strength as a function of a parameter including both voids and ineffective fiber is shown in figure 36(d). As can be seen, from figure 36(d), the voids have a very detrimental effect on the transverse strength of the composite. Experimental results are also shown in these figures. One point to be noted in figure 36(c) is that the ineffective fibers or the void at the interface have more severe effects at relatively low void volume ratios and level off as the void ratio increases.

The effects of voids on the intralaminar shear and longitudinal compressive strengths are illustrated in figures 37(a) and (b) and can be seen to be very significant. It was already mentioned that the intralaminar shear strength is a good measure of bond strength. Since this strength decreases as the void volume ratio increases, it implies that the bond strength at the interface is weakened by the presence of voids.

The effect of temperature on intralaminar shear strength has also been investigated. Some typical results are shown in figure 38 for a graphite fiber of 50×10^6-psi modulus, in an epoxy matrix with a fiber content of 50 percent. As can be seen from this figure, the intralaminar shear strength remains approximately invariant for temperatures ranging from -65° to 180° F. It decreases rather rapidly and approaches zero as the temperature reaches 350° F. It can be seen that the interface bond strength as measured by the intralaminar shear strength is insensitive to temperature rises to about one-half the cure temperature of the composite. Above this temperature, the interface bond becomes progressively weaker.

The effects of moist environment on the interface bond strength as measured by the shear fracture energy are illustrated in figure 39. The shear fracture energy is plotted

as a function of time in moist environments for two temperatures. As can be seen, the moisture has damaging effects on the interface bond, and these effects become more pronounced as the temperature is increased. Additional results on moist environments are reported in reference 50.

The results discussed in this section illustrate that the interfacial bond is sensitive to the fabrication process as indicated by the presence of voids. It is also sensitive to elevated-temperature environments, that is, those temperature levels which are greater than about one-half the cure temperature of the composite. Moisture also has damaging effects on interface bond, and these effects become more pronounced as the composite temperature is increased.

DESIGNING COMPOSITES WITH SPECIFIED BOND STRENGTH

It is possible to select constituent materials and process them such that the interfacial bond will be sufficient to yield a composite of expected structural integrity. Several factors could be used as an aid in selecting constituents to yield composites with specified bond strength. Some of these factors are described in this section.

The fiber diameter is an important variable in fiber composites. This variable seems to have no effect on interface bond strength, as is illustrated in figure 40.

The fiber content is a very significant parameter in designing fiber composites. And as already has been discussed, the stress concentrations at the interface may be strongly dependent on the fiber content. Fiber stresses produced by both external longitudinal applied loads and by thermal loads are illustrated in figures 41(a) and (b) as a function of the fiber volume ratio. As can be seen, the concentration effects of these stresses decrease rapidly with increasing fiber volume ratio. The critical length as a function of fiber content is shown in figure 41(c). It can be seen that critical length decreases very rapidly with increasing fiber volume ratio. The results in figure 41 illustrate that if the end use of the composite is to resist axial and thermal loads, the fiber volume ratio should be relatively high to minimize the stress concentrations. And in addition, the fibers used in such composites will be efficiently utilized since the critical length required is relatively small, as shown in figure 41(c).

The effect of constituent stiffness ratio E_f/E_m as a function of fiber content on the matrix or interface shear stress concentration is illustrated in figure 42. As can be seen in this figure, the shear stress concentration increases with decreasing fiber modulus. This increase becomes more pronounced at relatively high fiber volume ratios, for example, greater than 75 percent. Here again, to minimize the shear stress concentration, constituent materials should be selected with relatively high stiffness ratios.

In figure 43, the maximum thermally induced shear stress concentration is plotted

as a function of fiber volume ratio for three constituent material stiffness ratios. The results indicate that the shear stress concentration increases as the relative stiffness of the constituents decreases. To minimize these shear stresses and to enhance interfacial bond integrity, constituents should be selected with relatively high stiffness ratios.

A parameter which could be used in designing composites with specified bond strength is illustrated in figure 44(a). This parameter is called the debonding parameter and is the ratio of the shear strain magnification factor and the composite shear modulus. The debonding parameter is plotted in figure 44(a) as a function of matrix modulus for a fiber content of 0.5 and as a function of fiber content for a matrix modulus of 0.5×10^6 psi. It varies only slightly with fiber content. The debonding parameter shows a marked dependence on matrix modulus for moduli less than 0.5×10^6 psi. The results of figure 44(a) indicate that composites with low values of this ratio tend to have high bond strength. It can be seen in figure 44(b) that composites with higher intralaminar shear strength exhibit higher transverse impact energy. This condition corresponds to low values of the debonding parameter.

Another parameter which can be used in designing composites with specified bond strength is the energy-absorbing capability of the interface bond and the matrix in the vicinity of the fiber break (refs. 51 and 52). Photomicrographs of fiber fractures and corresponding schematics of energy-dissipation paths are illustrated in figure 45 for a boron fiber in epoxy. It can be seen in figure 45 that constituent materials can be selected to make composites with high energy-absorbing capability. Poor interface bonds and matrices exhibiting multipath fractures provide high energy-absorbing mechanisms.

The discussion of this section clearly indicates that certain methods can be used to select constituents which will result in specified interfacial bonding conditions. The type of load condition and the end use should be kept in mind in selecting constituent materials. The cardinal rule in designing with fiber composites is the following: The most suitable composite will evolve from the best possible compromise of all the competing factors.

CONCLUDING REMARKS

This review and discussion of the literature to assess the role of the fiber/matrix interface on composite structural integrity leads to the following conclusions:

1. Strong interface bond results in a composite with higher stiffness and higher static strength. However, it leads to more brittle and more notch-sensitive composites. A suitable compromise of the two is required in actual designs.

2. Several direct test methods have been developed to measure the stress state at the interface and the bond strength. The photoelastic method of multifiber inclusion is

17

the most reliable to determine point stress states. The fiber pullout test method is the most convenient for average bond strength. Fracture energy test methods are suitable for the initiation of debonding at the end of the fiber.

3. The interface bond strength can be assessed indirectly by the short-beam shear and transverse tensile test methods. The dynamic modulus and/or the log decrement are suitable for determining interface bond damage. The short-beam shear and the dynamic test methods are convenient for quality control and for determining environmental effects.

4. Analytical methods have been advanced to investigate the stress state at the interface. These methods include mechanics of materials, classical elasticity, and finite element. The finite element method is the most versatile and can handle a variety of boundary conditions. Predicted magnitudes of stress concentrations depend on the boundary conditions.

5. Theoretical results show that the shear stress concentration at fiber ends depends on fiber volume ratio, constituent stiffness ratio, and fiber end geometry. They show that the radial stress at the interface varies along the circumference and can be tensile or compressive depending on the sense of the thermal load and on the sense and direction of the mechanical load. Therefore, several degrees of freedom exist to obtain suitable interface bond for specific designs.

6. The presence of voids and moisture at the interface weaken the bond, as does elevated temperature. This weakening is detrimental to composite stiffness and strength in general.

7. The debonding parameter is a measure of local matrix shear-strain magnification and composite shear modulus. This parameter can be used to guide the selection of constituents for a specific interface bond in certain composite applications.

Lewis Research Center,
    National Aeronautics and Space Administration,
        Cleveland, Ohio, September 20, 1971,
            134-14.

18

APPENDIX - SYMBOLS

a	ellipse major axis
b	ellipse minor axis
d	diameter
E	normal modulus
G	shear modulus
G_{II}	interfacial bond shear fracture energy
k	volume ratio
$\bar{k}$	actual volume ratio
$\bar{k}_{if}$	actual volume ratio of ineffective fibers
k_v	void content
L	length
L_c	fiber critical or ineffective length
R	radius
r	coordinate
S	strength; subscripts define material, surface, direction, and sense
$\mathcal{S}_n$	cumulative probability
s	fiber spacing
ΔT	temperature difference
t	ply thickness
x,y,z	Cartesian coordinate system
r,θ,z	cylindrical coordinate system
α	thermal coefficient of expansion
γ	fracture energy
Δ	log decrement
δ	interface spacing
ϵ	strain; subscripts indicate material, surface, and direction
ν	Poisson's ratio; subscripts define load direction and displacement direction
σ	stress; subscripts indicate material, surface, and direction

σ_0 interface pressure on a single inclusion in an infinite medium

$\varphi_{\mu 12}$ matrix shear-strain magnification factor

$\varphi_{\mu 22}$ matrix transverse-strain magnification factor

$1, 2, 3$ material axes

Subscripts:

av	average
B	bond property
C	compression
f	fiber property
l	ply property
m	matrix property
r	radial direction
S	shear stress
T	tensile
v	void
z	direction
θ	coordinate direction
1	coordinate or property along fiber
2	coordinate or property transverse to fiber

Superscript:

(0)	initial properties

REFERENCES

1. Dietz, A. G. H.: Micromechanics of Fibrous Composites. Rep. MAB-207-M, Materials Advisory Board, National Academy of Science, May 1965.

2. Anon.: Ad Hoc Committee on Interface Problems in Fibrous Composites. Rep. MAB-214-M, Materials Advisory Board, National Academy of Science, Nov. 1965. (Available from DDC as AD-630256.)

3. Anon.: Interfaces in Composites. Spec. Tech. Publ. No. 452, ASTM, 1969.

4. Bascom, W. D.: Water at the Interface. Proceedings of the 25th Annual Technical Conference, Society of the Plastics Industry, 1970, pp. 13-C, 1 to 13-C, 12.

5. Broutman, Lawrence J.: Mechanical Requirements of the Fiber-Matrix Interface. Proceedings of the 25th Annual Technical Conference, Society of the Plastics Industry, 1970, pp. 13-B, 1 to 13-B, 8.

6. Erickson, Porter W.: Historical Background of the Interface: Studies and Theories. Proceedings of the 25th Annual Technical Conference, Society of the Plastics Industry, 1970, p. 13-A, 1.

7. Plueddemann, Edwin P.: Adhesion Through Silane Coupling Agents. Proceedings of the 25th Annual Technical Conference, Society of the Plastics Industry, 1970, pp. 13-D, 1 to 13-D, 10.

8. Scola, D. A.; and Brooks, C. S.: Surface Aspects of New Fibers, Boron, Silicon Carbide, and Graphite. Proceedings of the 25th Annual Technical Conference, Society of the Plastics Industry, 1970, pp. 13-F, 1 to 13-F, 18.

9. Kelly, A.: Interface Effects and the Work of Fracture of a Fibrous Composite. Rep. NPL-IMS-10, National Physical Lab., Feb. 1970.

10. Broutman, L. J.; and Sahu, S.: The Effect of Interfacial Bonding on the Toughness of Glass Filled Polymers. Proceedings of the 26th Annual Technical Conference, Society of the Plastics Industry, 1971, pp. 14-C, 1 to 14-C, 14.

11. McGarry, F.; and Fujiwara, M.: Glass Fiber-Resin Bond Studies. Proceedings of the 23rd Annual Technical Conference, Society of the Plastics Industry, 1968, p. 9-B, 1.

12. Koeneman, James B.: Interfiber Failure of Composite Materials. Division of Solid Mechanics, Structures and Mechanical Design. Rep. 38, School of Eng., Case Western Reserve Univ., Dec. 1969.

13. Outwater, John O.; and Murphy, Michael C.: On the Fracture Energy of Uni-Directional Laminates. Proceedings of the 24th Annual Technical Conference, Society of the Plastics Industry, 1969, pp. 11-C, 1 to 11-C, 8.

14. MacLaughlin, Thomas F.: A Photoelastic Analysis of Fiber Discontinuities in Composite Materials. J. Composite Mat., vol. 2, 1968, pp. 44-55.

15. Schuster, D. M.; and Scala, E.: Mechanical Interactions in Fiber Reinforced Photoelastic Composites. Fundamental Aspects of Fiber Reinforced Plastic Composites. R. T. Schwartz and H. S. Schwartz, eds., Interscience Pub., 1968, pp. 45-62.

16. Marloff, R. H.; and Daniel, I. M.: Three-Dimensional Photoelastic Analysis of a Fiber-Reinforced Composite Model. Experiment. Mech., vol. 9, no. 4, Apr. 1969, pp. 156-162.

17. Koufopoulos, T.; and Theocaris, P. S.: Shrinkage Stresses in Two-Phase Materials. J. Composite Mat., vol. 3, Apr. 1969, pp. 308-320.

18. Theocaris, P. S.; and Marketos, E.: Shrinkage Stress Concentrations In-Plane Two-Phase Systems. Fibre Sci. & Tech., vol. 3, 1970, p. 21.

19. Holister, G. S.; and Thomas, C.: Fibre Reinforced Materials. Elsevier Publishing Co., Ltd., 1966.

20. Tarnopol'skiy, Yu. M.; and Skudra, A. M.: Construction Strength and Deformation Properties of Fiber Glass Reinforced Plastics. Rep. FRDL-T-1875-66, Inst. Modern Languages, Inc. (TT-67-60676, AD-645948), Dec. 1966.

21. Amirbayat, J.; and Hearle, J. W. S.: Properties of Unit Composites as Determined by the Properties of the Interface. Part I: Mechanism of Matrix-Fibre Load Transfer. Fibre Sci. & Tech., vol. 2, 1969, p. 123.

22. Amirbayat, J.; and Hearle, J. W. S.: Properties of Unit Composites as Determined by the Properties of the Interface. Part II: Effect of Fibre Length and Slippage on the Modulus of Unit Composites. Fibre Sci. & Tech., vol. 2, 1969, p. 153.

23. Amirbayat, J.; and Hearle, J. W. S.: Properties of Unit Composites as Determined by the Properties of the Interface. Part III: Experimental Study of Unit Composites without a Perfect Bond between the Phases. Fibre Sci. & Tech., vol. 2, 1970, p. 223.

24. Chamis, Christos C.: Design Oriented Analysis and Structural Synthesis of Multi-layered Filamentary Composites. Ph. D. Thesis, Case Western Reserve University, 1967.

25. Chamis, Christos C.: Failure Criteria for Filamentary Composites. NASA TN D-5367, 1969.

26. Bloom, Joseph M.; and Wilson, Howard B., Jr.: Axial Loading of a Unidirectional Composite. J. Composite Mat., vol. 1, 1967, pp. 268-277.

27. Bloom, Joseph M.; and Adams, Donald F.: Axial Loading of a Unidirectional Composite - Anisotropic Filaments. J. Composite Mat., vol. 3, Jan. 1969, pp. 186-188.

28. Haener, Juan; Ashbaugh, Noel; Chia, Chuen-Yuan; and Feng, Ming-Yuan: Investigation of Micromechanical Behavior of Fiber Reinforced Plastics. Whittaker Corp. (USAAVLABS-TR-67-66, AD-667901), Feb. 1968.

29. Pickett, Gerald: Elastic Moduli of Fiber Reinforced Plastic Composites. Fundamental Aspects of Fiber Reinforced Plastic Composites. R. T. Schwartz and H. S. Schwartz, eds., Interscience Publ., 1968, pp. 13-27.

30. Adams, Donald F.; Doner, Douglas R.; and Thomas, Rodney L.: Mechanical Behavior of Fiber-Reinforced Composite Materials. Rep. U-4093, Aeronautic (AFML-TR-67-96, AD-654056), May 1967.

31. Leissa, A. W.; and Clausen, W. E.: Application of Point Matching to Problems in Micromechanics. Fundamental Aspects of Fiber Reinforced Plastic Composites. R. T. Schwartz and H. S. Schwartz, eds., Interscience Publ., 1968, pp. 29-44.

32. Chang, C. S.; and Conway, H. D.: Bond Stresses in Fiber Reinforced Composites Subjected to Uniform Tension. J. Composite Mat., vol. 2, 1968, pp. 168-185.

33. Conway, H. D.; Chu, W. W.; and Chang, C. I.: Effect on Bond Stresses of Partial Bond Failure of Overlapping Fibers in a Composite Material. Fibre Sci. & Tech., vol. 2, 1970, p. 289.

34. Sadowsky, M. A.; Hsu, Y. C.; and Hussain, M. A.: Effect of Couple-Stresses on Force Transfer Between Embedded Microfibers. J. Composite Mat., vol. 1, 1967, pp. 174-187.

35. Carrara, S.; and McGarry, F.: Matrix and Interface Stresses in a Discontinuous Fiber Composite Model. J. Composite Mat., vol. 2, 1968, pp. 222-243.

36. Foye, Raymond L.; and Baker, Donald J.: Design/Analysis Methods for Advanced Composite Structures. North American Rockwell Corp. (AFML-TR-70-299, vol. I, AD-88-2626), Feb. 1971.

37. Foye, Raymond L.; and Baker, Donald J.: Design/Analysis Methods for Advanced Composite Structures. North American Rockwell Corp. (AFML-TR-70-299, vol. II, AD-88-2627), Feb. 1971.

38. Iqbal, Mohammed A.; and Krokosky, Edward M.: Interaction Stresses in Composite Systems. ASCE J. Eng. Mech., vol. 96, no. EM-6, Dec. 1970, pp. 825-845.

39. Remedios, N. C.; and Wood, W. G.: Stress Transfer from a Loaded Matrix to a Single Fiber. J. Composite Mat., vol. 2, 1968, pp. 517-520.

40. Chamis, C. C.; and Sendeckyj, G. P.: Critique on Theories Predicting Thermoelastic Properties of Fibrous Composites. J. Composite Mat., vol. 2, 1968, pp. 332-359.

41. Wadsworth, N. S.; and Spilling, I.: Load Transfer from Broken Fibres in Composite Materials. Brit. J. Appl. Phys., Ser. 2, vol. 1, no. 8, Aug. 1968, pp. 1049-1058.

42. Amirbayat, J.; and Hearle, J. W. S.: Factors Affecting the Bond Failure in Unit Composites. Fibre Sci. & Tech., vol. 3, 1970, p. 147.

43. Hancock, P.; and Cuthbertson, R. C.: The Effect of Fibre Length and Interfacial Bond in Glass Fibre-Epoxy Resin Composites, J. Materials Sci., vol. 5, Sept. 1970, pp. 762-768.

44. Outwater, J. O.; and Murphy, M. C.: Fracture Energy of Unidirectional Laminates. Modern Plastics, vol. 47, no. 9, Sept. 1970, p. 160.

45. Outwater, J. O.; and Murphy, M. C.: The Influence of Environment and Glass Finishes on Fracture Energy of Glass-Epoxy Joints. Proceedings of the 25th Annual Technical Conference, Society of the Plastics Industry, 1970, p. 16-D,1.

46. Schrader, M. E.: Radioisotopic Studies of Bonding at the Interface. Proceedings of the 25th Annual Technical Conference, Society of the Plastics Industry, 1970, pp. 13-E, 1 to 13-E, 6.

47. Stone, M. H.: Bond Degradation by Liquids. Composites, vol. 1, Mar. 1970, pp. 164-166.

48. Zurbrick, John R.: Nondestructive Testing of Glass Fiber-RP: Key to Composition Characterization and Design Properties Prediction. SPE J., vol. 24, no. 9, Sept. 1968, pp. 56-60.

49. Doner, D. R.; and Novak, R. C.: Structural Behavior of Laminated Graphite Filament Composites. Proceedings of the 24th Annual Technical Conference, Society of the Plastics Industry, 1969, pp. 2-D, 1 to 2-D, 8.

50. Wyatt, R. C.; and Ashbee, Kenneth, H. G.: Debonding in Carbon Fibre/Polyester Resin Composites Exposed to Water: Comparison with "E" Glass Fibre Composites. Fibre Sci. & Tech., vol. 2, no. 1, 1969, pp. 29-39.

51. Mullin, J. W.; Berry, J. M.; and Gatti, A.: Some Fundamental Fracture Mechanisms Applicable to Advanced Filament-Reinforced Composites. J. Composite Mat., vol. 2, 1968, pp. 82-103.

52. Mullin, J. V.; and Mazzio, V. F.: Basic Failure Mechanisms in Advanced Composites. Final Report to NASA, Cont. No. NASW-2083 (April 1971).

53. Weeton, J. W.; and Signorelli, R. A.: Fiber-Metal Composites. Strengthening Mechanisms: Metals and Ceramics. J. J. Burke, N. L. Reed, and Volker Weiss, eds., Syracuse University Press, 1966, pp. 477-530.

54. Chamis, Christos C.; Hanson, Morgan P.; and Serafini, Tito T.: Designing for Impact Resistance With Unidirectional Fiber Composites. NASA TN D-6463, 1971.

55. Jech, Robert W.: Influence of Fiber Aspect Ratio on the Stress-Rupture Life of Discontinuous Fiber Composites. NASA TN D-5735, 1970.

56. Marloff, R. H.; and Daniel, I. M.: Three-Dimensional Photoelastic Analysis of a Fiber-Reinforced Composite Model. Experimental Mech., vol. 9, Apr. 1969, pp. 156-162.

57. Elkin, R. A.; Fust, G.; and Hanley, D. P.: Characterization of Graphite Fiber/ Resin Matrix Composites. Composite Materials: Testing and Design. Spec. Tech. Publ. No. 460, ASTM, 1969, pp. 321-335.

58. Lifshitz, J. M.; and Rotem, A.: Determination of Reinforcement Unbonding of Composites by a Vibration Technique. J. Composite Mat., vol. 3, July 1969, pp. 412-423.

59. Greszczuk, Longin B.: Micromechanics Failure Criteria for Composites Subjected to Transverse Normal Loading. Paper 71-355, AIAA, Apr. 1971.

60. Daniels, B. K.; Harakas, N. K.; and Jackson, R. C.: Short Beam Shear Tests of Graphite Fiber Composites. Fibre Sci. & Tech., vol. 3, 1971, p. 187.

TABLE I. - COMBINED STRESSES AT INTERFACES OF TYPICAL FIBER/RESIN COMPOSITES (REF. 5)
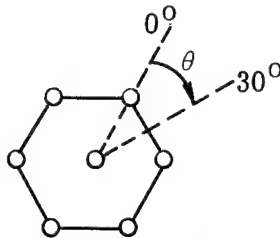
Fiber volume ratio, k_f	Fiber/ matrix modulus ratio, E_f/E_m	Radial tensile stress, σ_{rr}, psi		Maximum resin hoop stress $(\theta = 30^O)$, $\sigma_{\theta\theta, max}$, psi	Maximum circumferential shear stress, $\sigma_{r\theta, max}$, psi
		$\theta = 0^O$	$\theta = 30^O$		
Shrinkage stresses (resin shrinkage, 1 percent)					
0.64	150	-2000	500	5 000	1000
.64	26	-2500	500	5 000	↓
.70	150	-2000	1000	6 000	
.70	26	-3000	1000	6 000	
Stresses due to longitudinal tensile stress (σ_{l11}, 100 000 psi)					
0.64	150	-700	400	7 500	1500
.64	26	-1000	1000	7 500	2000
.70	150	-1200	1000	9 000	2500
.70	26	-1300	1300	9 000	2500
Combined stresses					
0.64	150	-2700	900	12 500	2500
.64	26	-3500	1500	12 500	3000
.70	150	-3200	2000	15 000	3500
.70	26	-4300	2300	15 000	3200
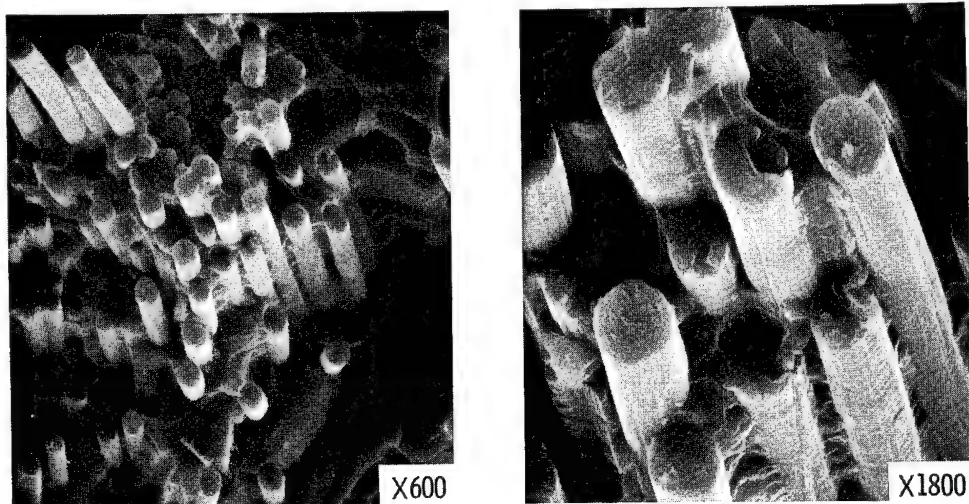
Figure 1. – Photomicrographs of fracture surface showing interfaces and fiber pullout. Fortafil 5-Y P10P composite.
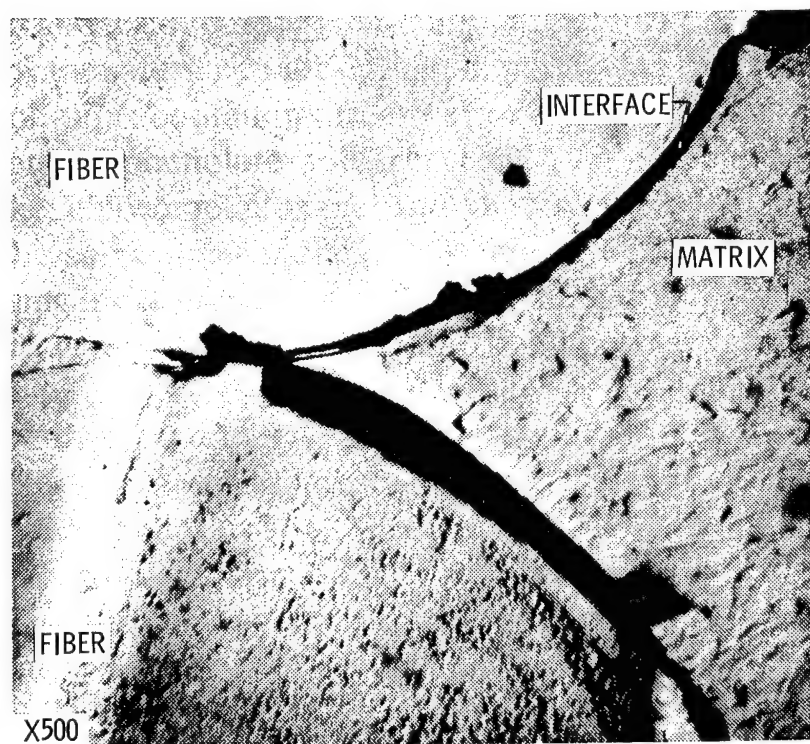
Figure 2. – Crack initiation where filaments come into contact. Specimen loaded to 80 percent of compressive strength for 16 hours. (From ref. 5.)
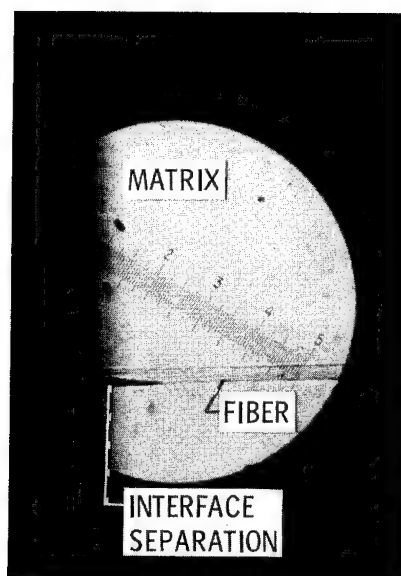
(a) Edge debonding of single fiber.
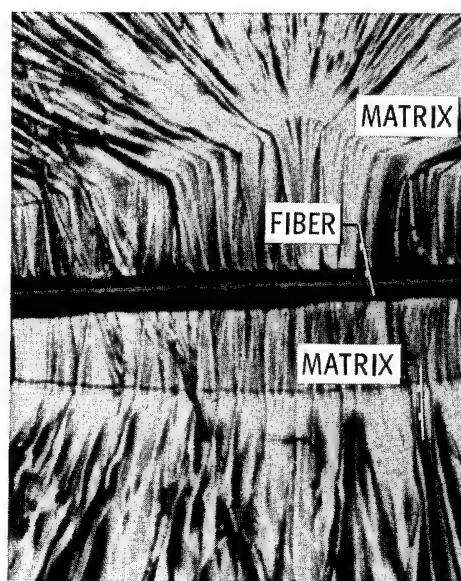
(b) Matrix fracture surface containing a single fiber.

Figure 3. – Debonding conditions at interface of model loaded in tension transverse to fiber. (From ref. 12.)
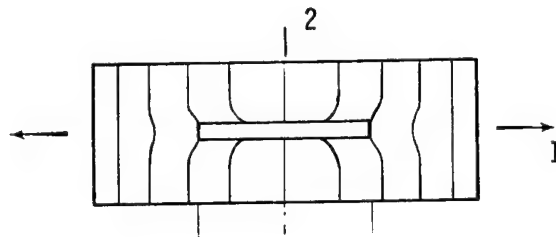
(a) Deformation model.
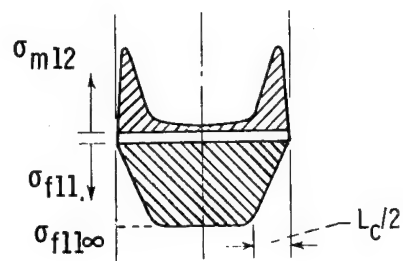
(b) Elastic.
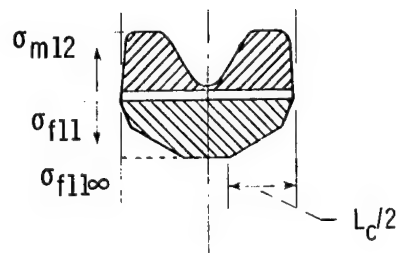
(c) Elastic-plastic.

Figure 4. - Stress distribution at the interface produced by elastic and elastic-plastic matrix. σ_{m12} denotes interfacial shear stress; σ_{f11} denotes fiber tensile stress. (From ref. 19.)
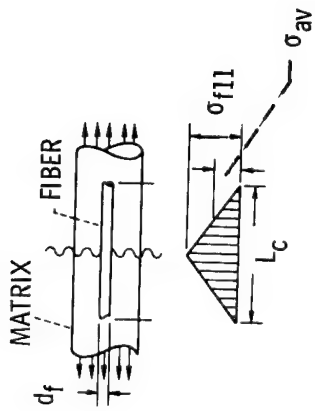
(a-1) Fiber of critical length; $L_c/d_f = 1/2 \, (\sigma_{f11}/\sigma_{m12})$.
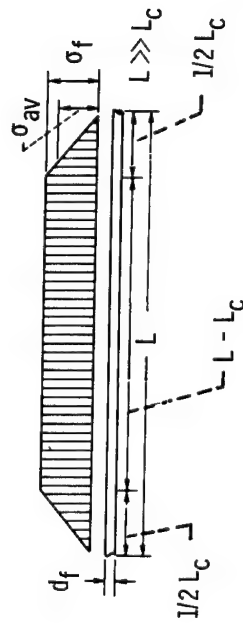
(a-2) Fiber much greater than critical length.

(a) Stress distribution in fibers.
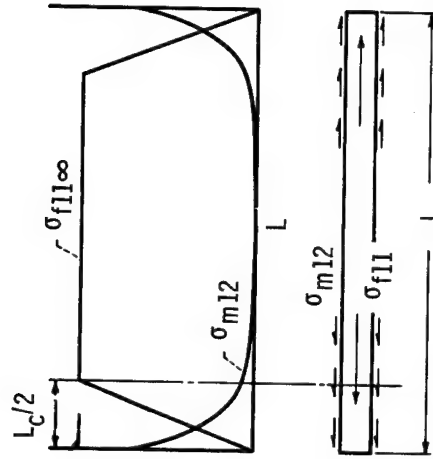
(b) Stress distribution within and on surface of fiber.

Figure 5. – Schematic illustrating stress distribution and term definitions at the interface. (From ref. 53.)
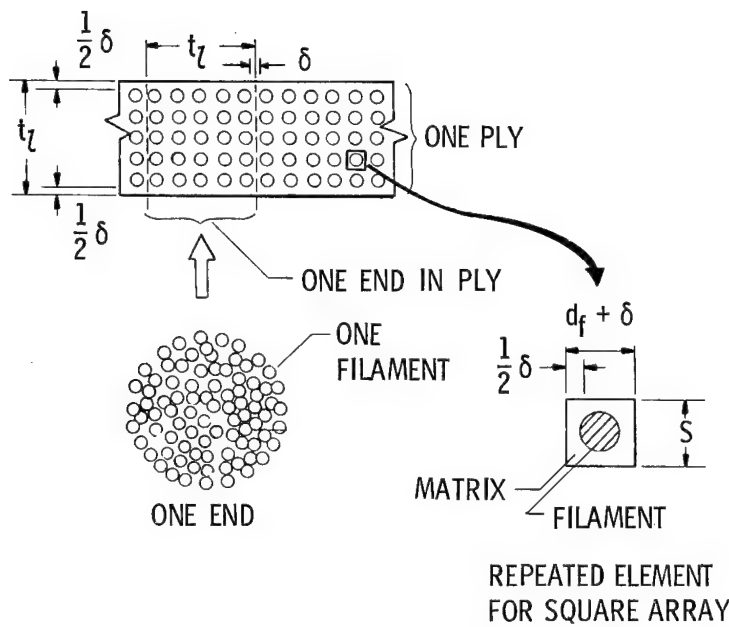
Figure 6. – Schematic of ply and repeating element. (From ref. 24.)
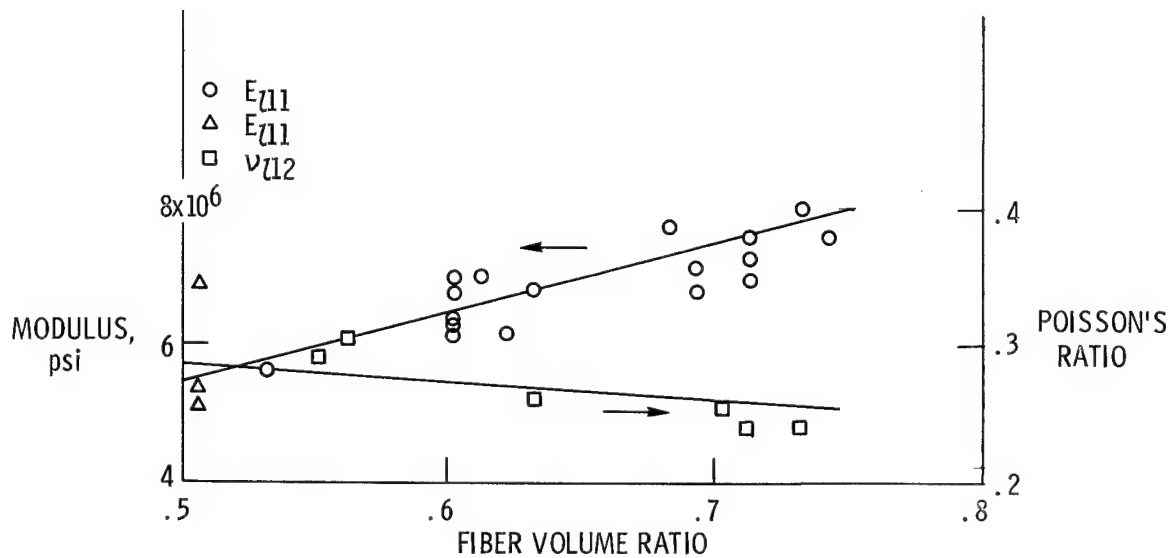
Figure 7. – Modulus and Poisson's ratio for E-glass/epoxy composites. (From ref. 24.)
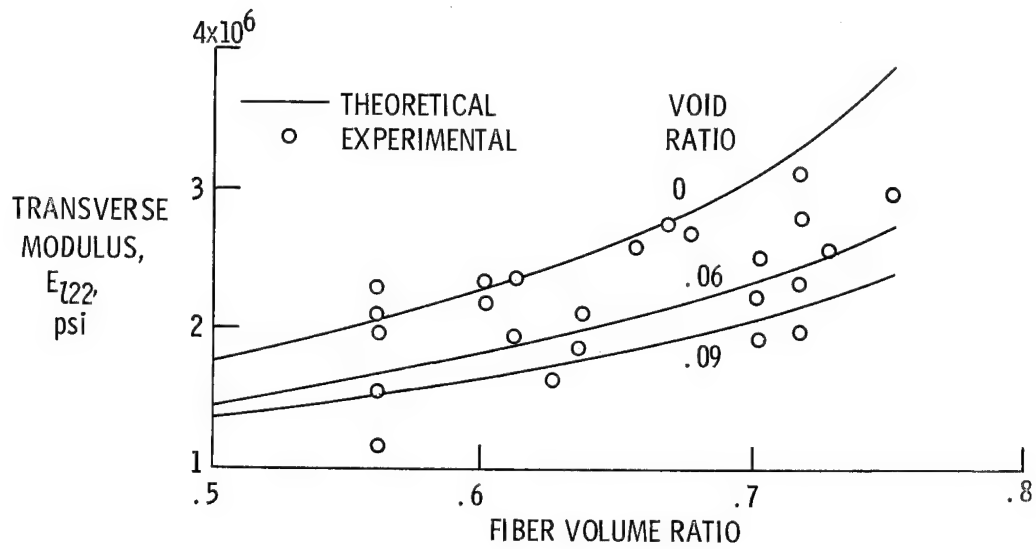
Figure 8. – Effect of voids on transverse modulus in E-glass/epoxy composites. (From ref. 24.)
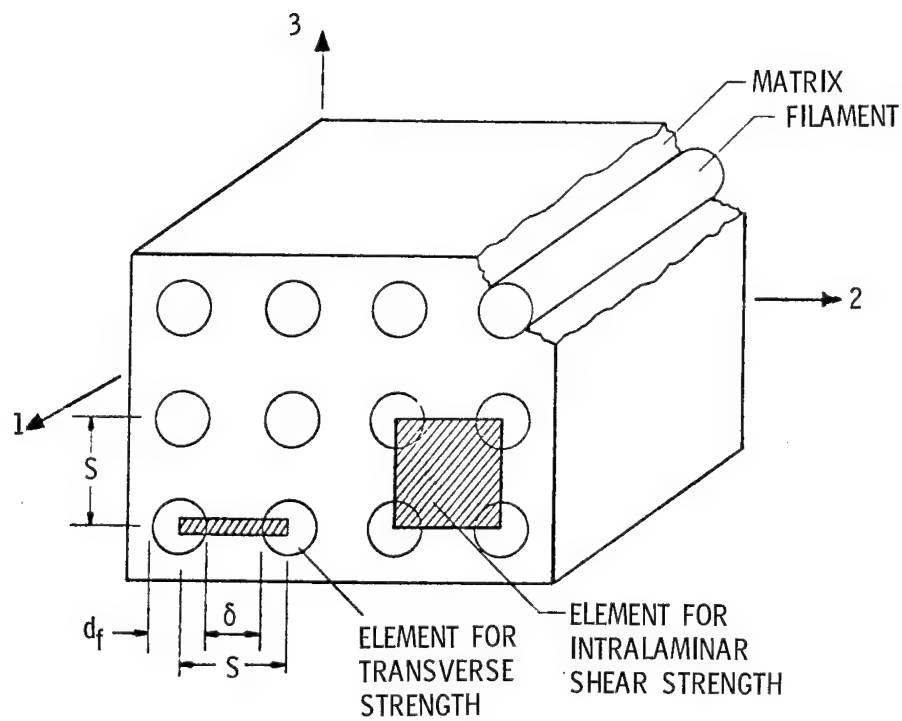
Figure 9. – Schematic of square array. (From ref. 24.)
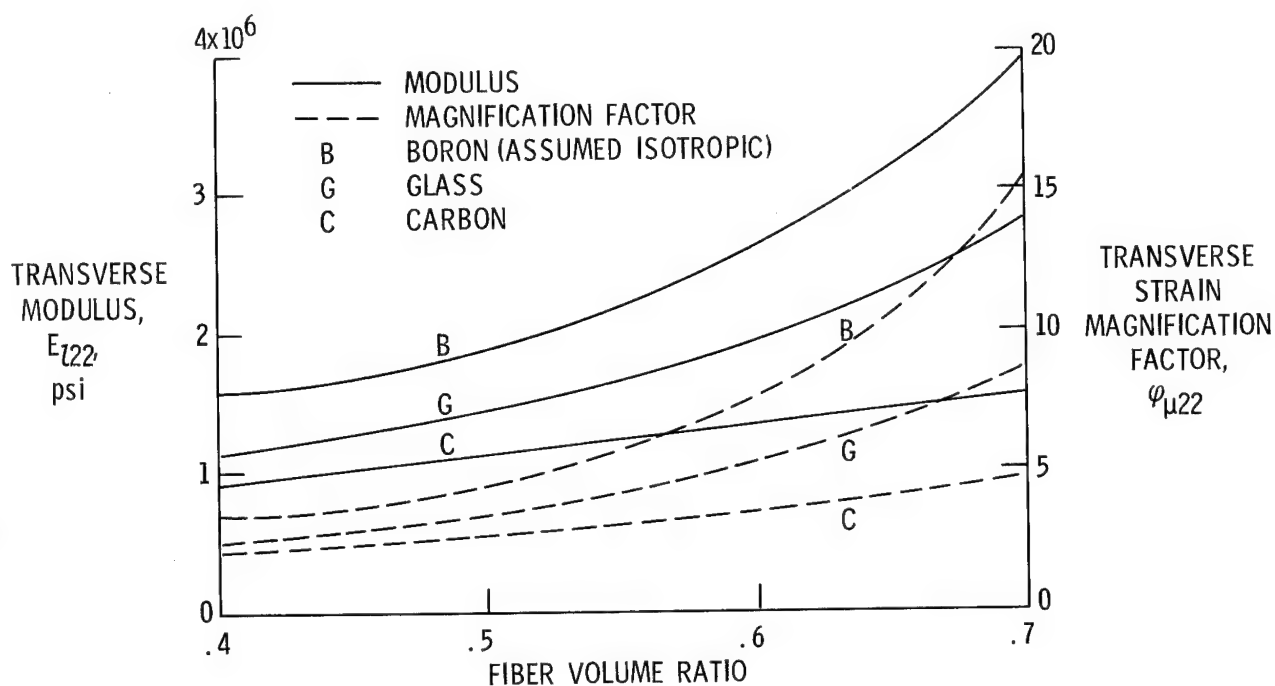
Figure 10. – Transverse modulus and strain magnification factor for three different filament/resin plies. (From ref. 24.)

(a) Brittle.   (b) Brittle with filament pullout.   (c) Irregular.
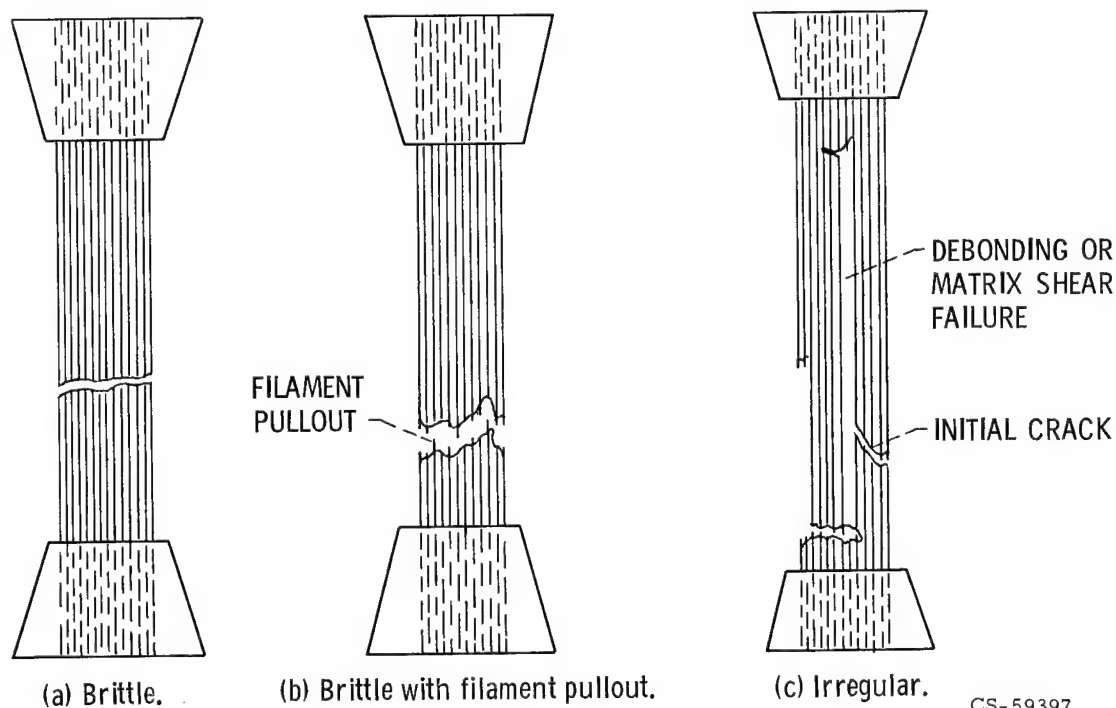
CS-59397

Figure 11. – Longitudinal tensile failure modes. (From ref. 24.)

33
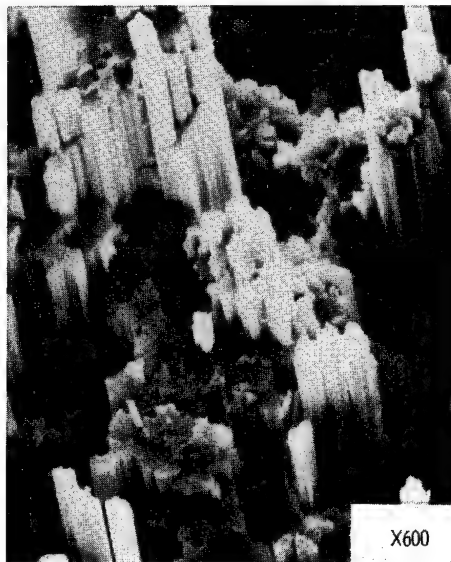
(a) Longitudinal fracture of Thornel-50S composite.

(b) Transverse fracture of Thornel-50S composite.
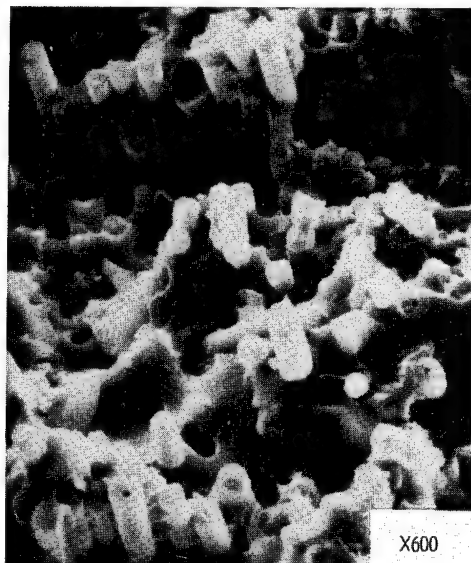
(c) Longitudinal fracture of high-tensile-strength composite.
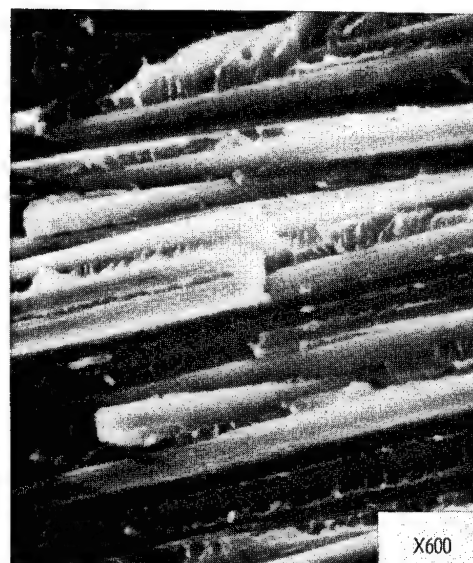
(d) Transverse fracture of high-tensile-strength composite.

Figure 12. – Scanning electron photomicrographs of fractured surfaces of graphite/epoxy composites. (From ref. 54.)
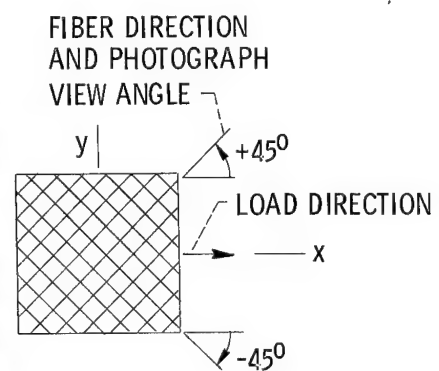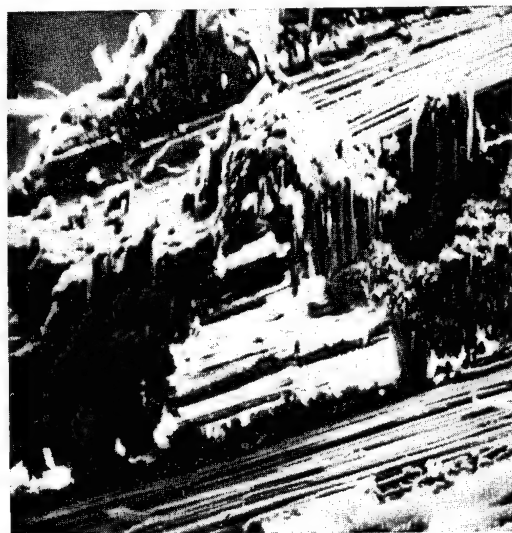
Figure 13. - Failure surface of five-layer +45⁰ Thornel-50S/epoxy composites (~x100). (From ref. 12).

GRIP — WIRE — BUTTON —

d_f

(MATRIX) —

L

A

A

SECTION A-A

(a) Test specimen.

△ WIRE FAILURE
○ PULLOUT

LOAD,
kg

15

10

5

┌ CRITICAL (L_c/d_f)

0   5   10   15

TEMPERATURE,
°C

○   649
□   816
OPEN SYMBOLS DENOTE
WIRE FAILURE
SOLID SYMBOLS DENOTE
PULLOUT

LOAD,
lbf

15

10

5

6   10   14   18   22   26   30

LENGTH/DIAMETER, L/d_f

(b) Failure load for tung-
sten fibers in copper
(room temperature).

(c) Failure load for tungsten
wire in copper (short-time
tensile tests).

Figure 14. - Schematic of fiber pullout test method and experi-
mental results. (From ref. 55.)
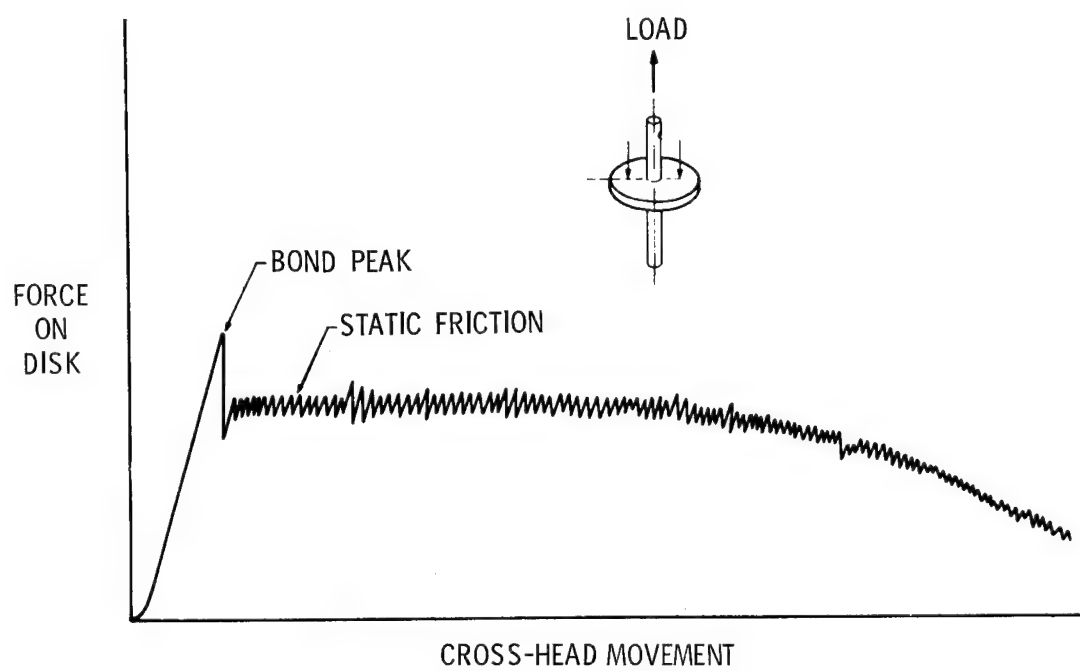
Figure 15. - Typical load-displacement curve for button-type test. (From ref. 5.)

0.5 IN. | 0.5 IN.

FIBER —— 1.5 IN.

SHEAR

FIBER —— 0.45-0.50 IN.

R = 1 IN. 1.5 IN.

0.25 IN.
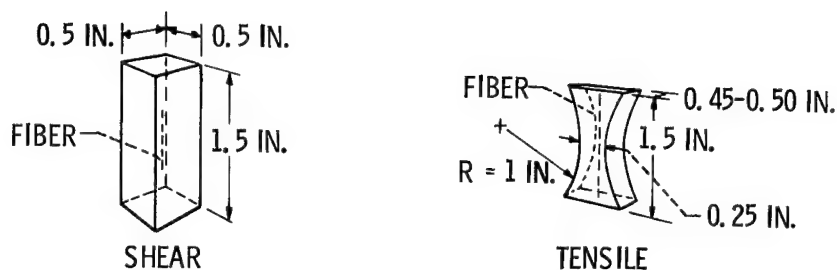
TENSILE

(a) Single-fiber specimens for interface shear and tensile strengths.

○ METHANOL TREATED; WATER BOIL   ○ UNTREATED; 356 K (180° F)
△ METHANOL TREATED; NO BOIL   △ UNTREATED; 356 K/422 K (180° F/300° F)
———— UNTREATED   ● METHANOL TREATED

CUMULATIVE PROBABILITY, $\mathcal{S}_n$

TENSILE STRENGTH, ksi
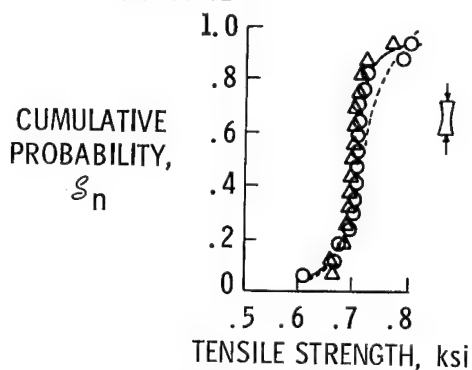
(b) Methanol-treated filament – effect of exposure.

SHEAR STRENGTH, ksi
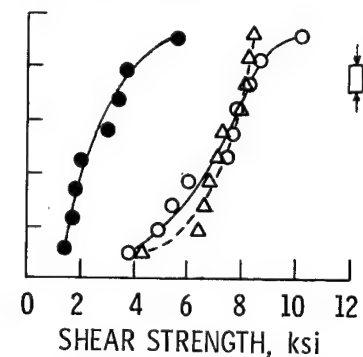
(c) Effect of filament treatment and resin cure.

Figure 16. – Model test methods for interface bond shear and tensile strengths – test results for boron fiber in epoxy. (From ref. 5.)

CODE	PRECURSOR	FIBER MODULUS, psi	FIBER DENSITY,	TWIST, TURNS/ in.	SURFACE TREATED	CROSS-SECTIONAL AREA OF FILAMENT, μm^2	NO. OF FILAMENT IN YARN
A	RAYON[a]	50×10^6	1.72	4	NO	27	1 440
B	RAYON[a]	↓	1.72	4	YES	27	↓
C	RAYON[b]		1.64	1.5	NO	32	
D	RAYON[b]		1.64	1.5	YES	32	
E	POLYACRYLONITRILE[c]	60	1.99	0	NO	60	10 000
F	POLYACRYLONITRILE[c]	60	1.99	0	YES	60	10 000
G	POLYACRYLONITRILE[d]	40	1.74	0	YES	60	10 000

[a] HITCO (H. I. THOMPSON & CO.) WITH DESIGNATION HMG-50.
[b] UNION CARBIDE CORP WITH DESIGNATION THORNEL 50.
[c] MORGANITE CO. WITH DESIGNATION MODMOR I.
[d] MORGANITE CO. WITH DESIGNATION MODMOR II.
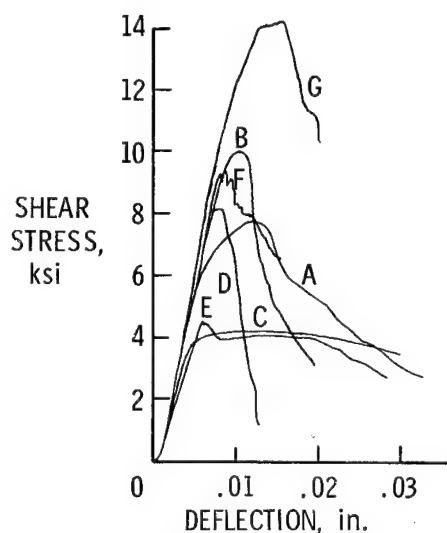
(a) Typical short-beam shear curves for fiber types shown in table. (From ref. 60.)
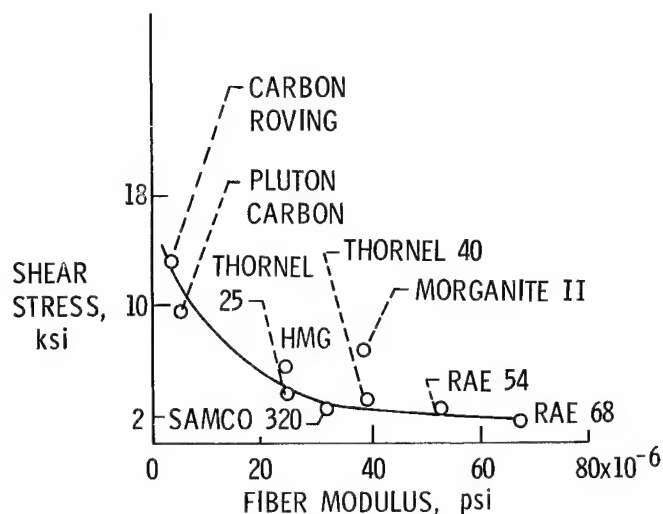
(b) Effects of fiber modulus on graphite fiber/epoxy composite shear strengths. (From ref. 3, p. 6.)

Figure 17. – Results of intralaminar shear strength test.
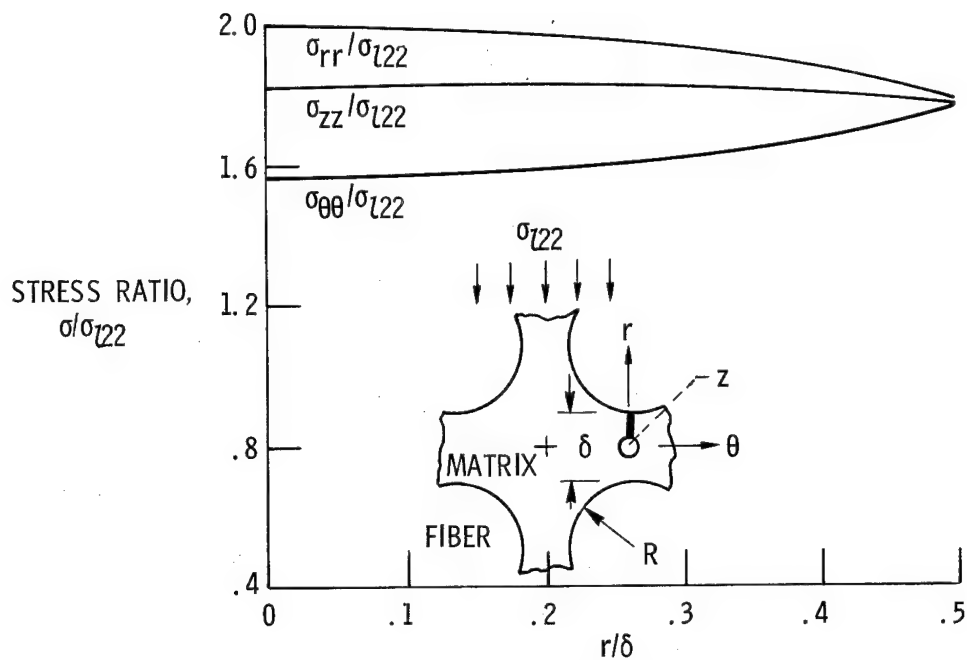
Figure 18. – Distribution of external load stresses across minimum section between fibers parallel to direction of applied load. Fiber volume ratio, ~0.5; δ/R = 0.5. (From ref. 56.)

(a) Transverse.
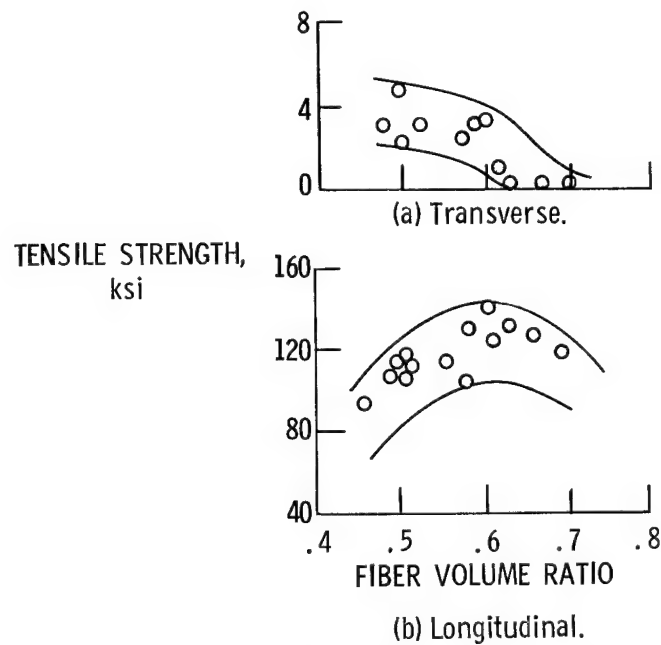
(b) Longitudinal.

Figure 19. – Transverse and longitudinal tensile strengths for Thornel-50/epoxy unidirectional composite. (From ref. 57.)
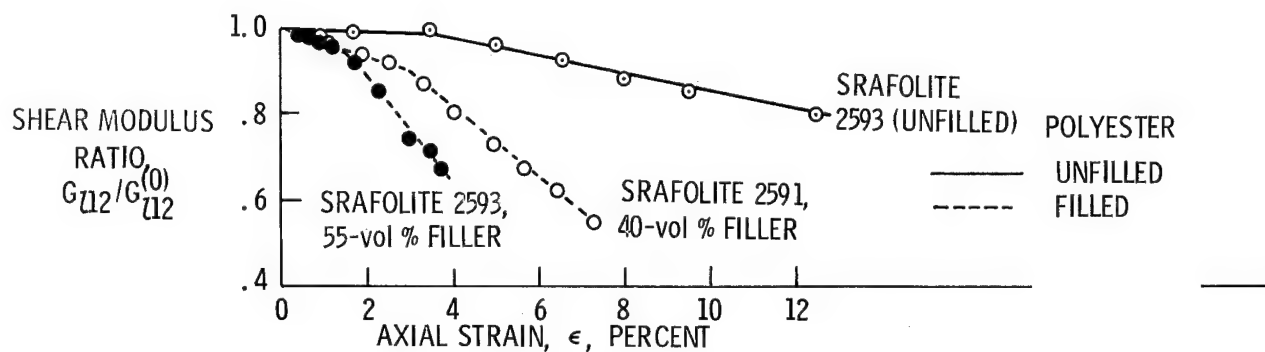
(a) Dynamic shear modulus; strain rate, 44.7×10^{-4} min^{-1}.
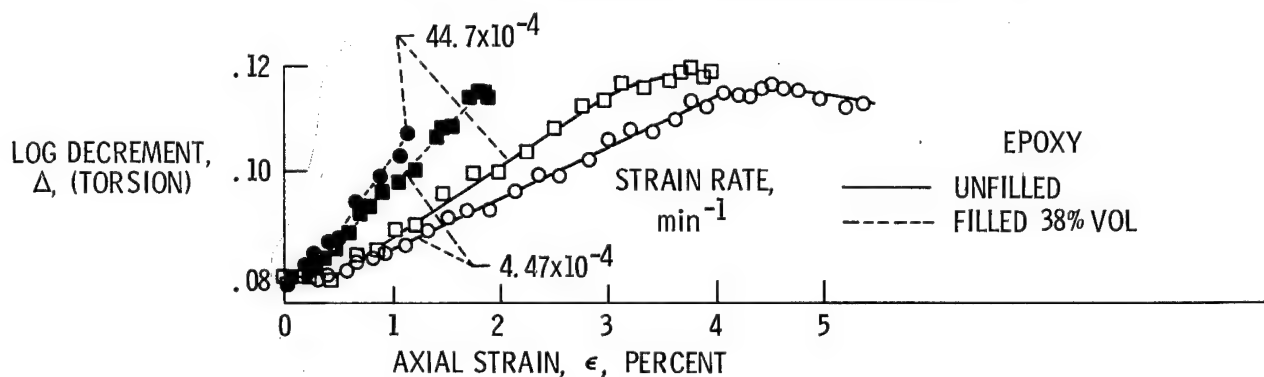
(b) Log decrement (damping of torsional vibrations).

Figure 20. - Results of dynamic modulus and log decrement test methods for particulate composites. (From ref. 58.)

41

(a) Model.

(b) Crack front in polarized light showing debonding of a filament.
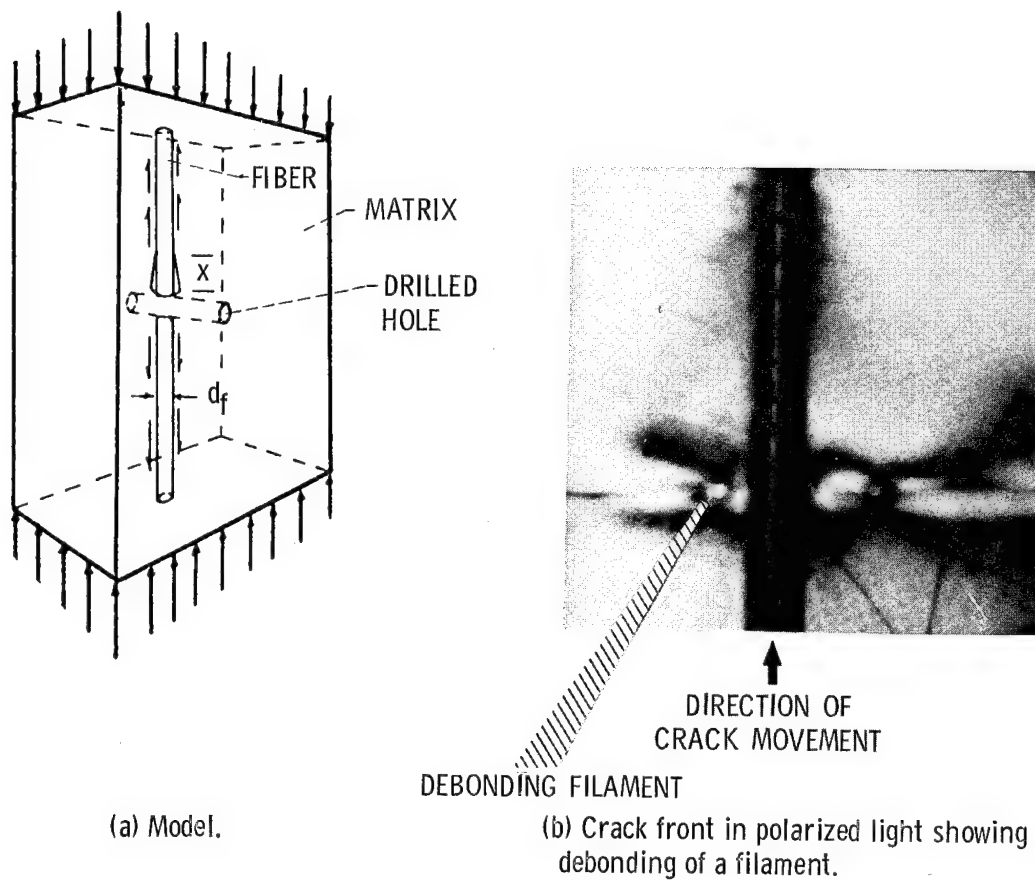
Figure 21. - Debonding shear fracture energy model. (From ref. 44.)
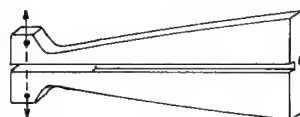
(a) Tapered double-cantilever cleavage specimen.
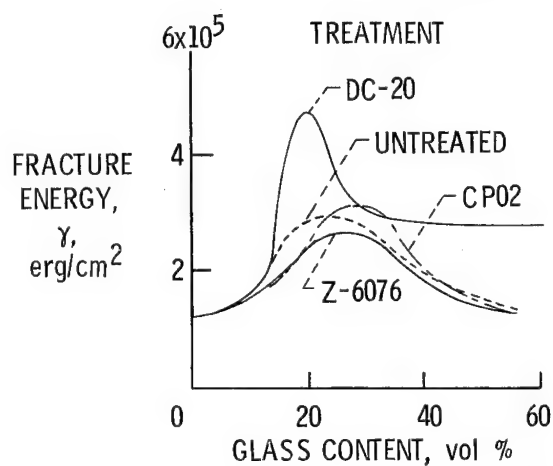
(b) Average fracture initiation energy against volume percent glass.
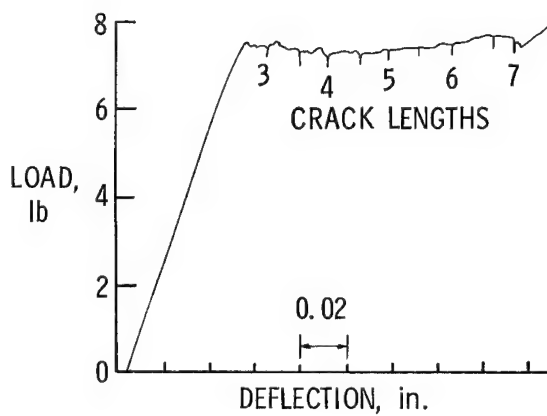
(c) Force against deflection for continuous crack propagation. CP02 treatment; 50-volume-percent glass.

Figure 22. - Double-cantilever cleavage model and results for particulate glass/epoxy composites. (From ref. 10.)
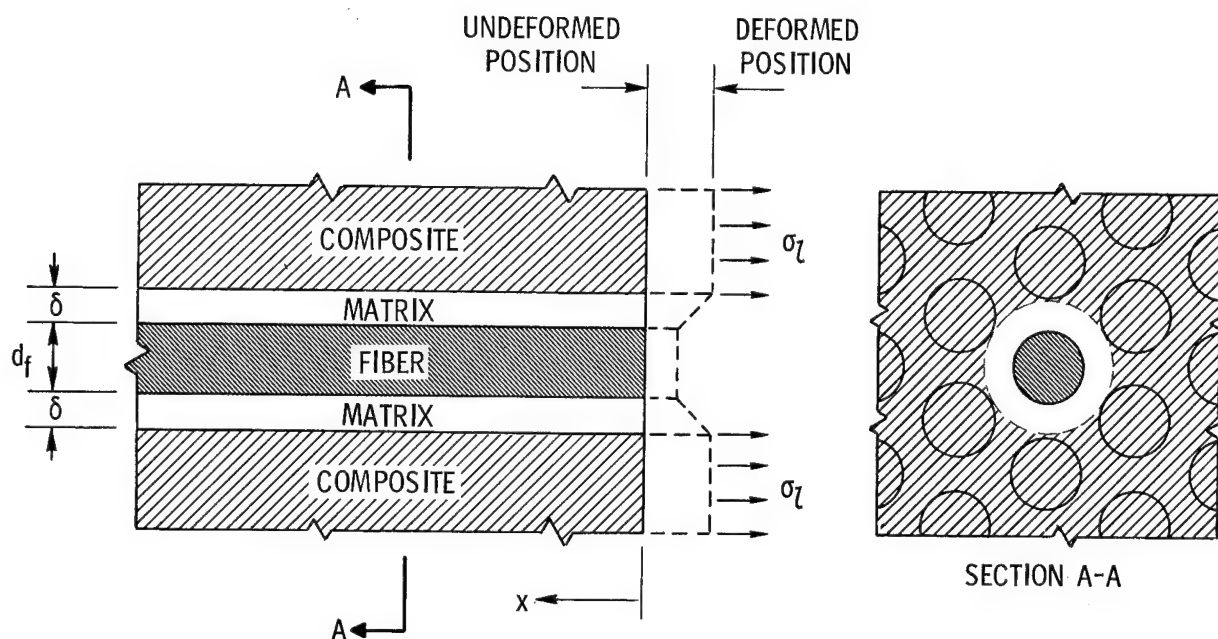
Figure 23. – Schematic of mechanism of longitudinal load transfer in fiber composites.
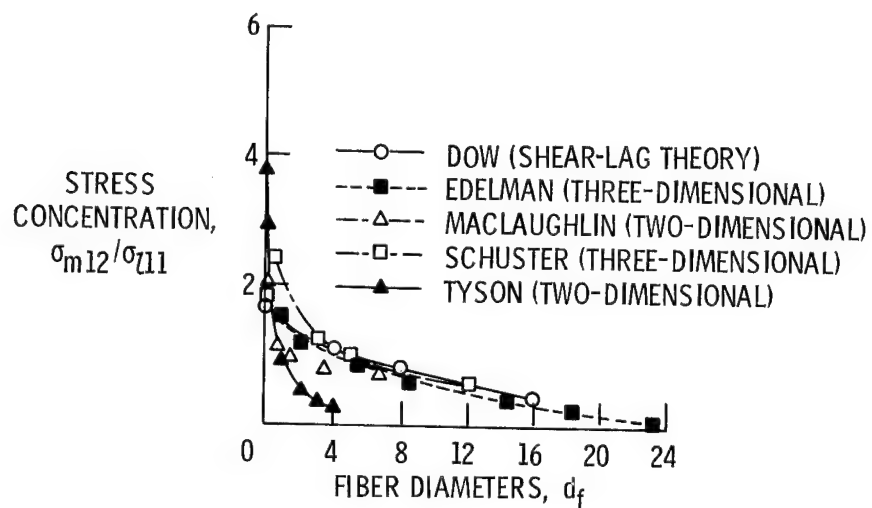
Figure 24. – Shear stress along matrix/fiber interface, as determined by five different investigators for tensile loading. (From ref. 5.)

44
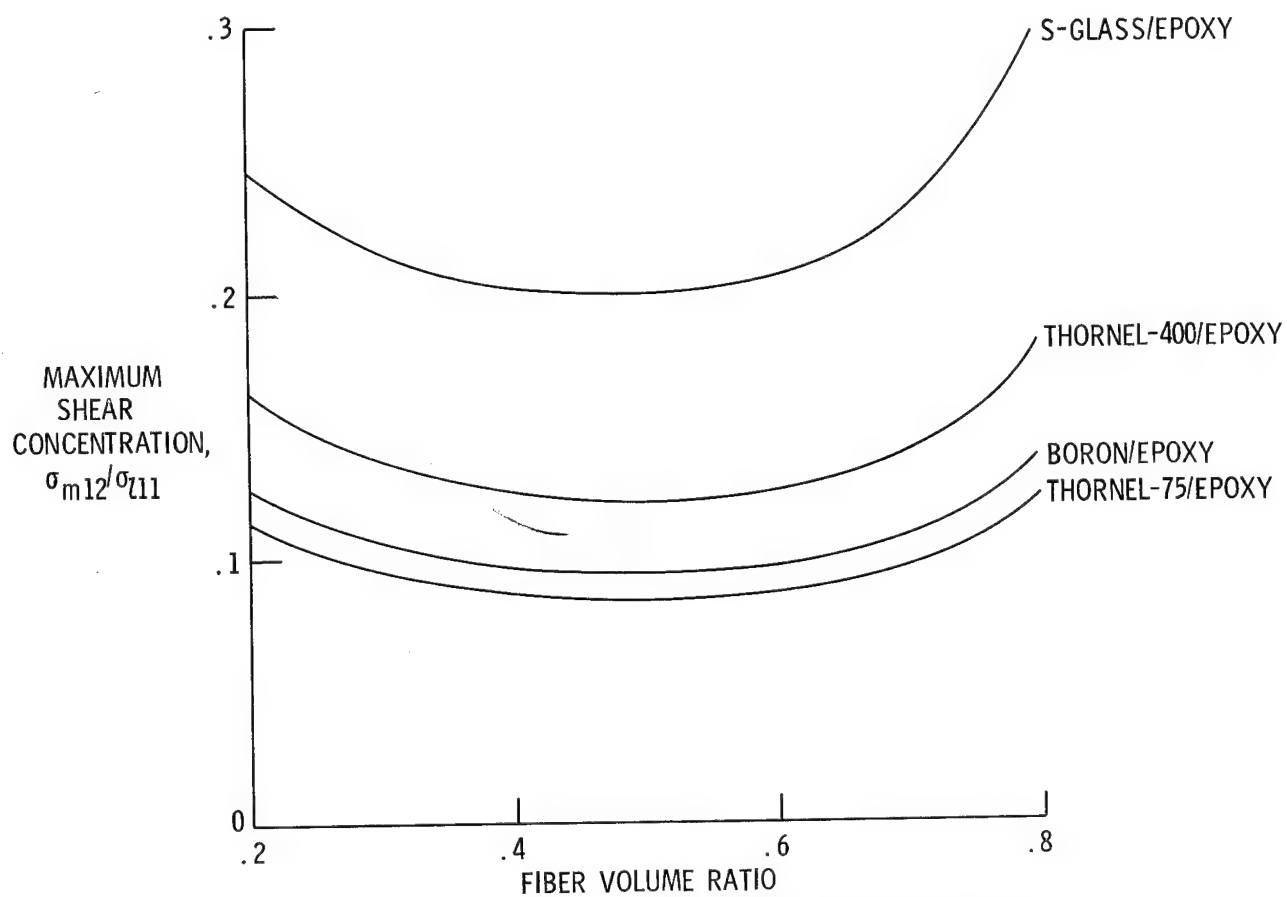
Figure 25. - Maximum shear concentration at interface due to axial tensile load. Matrix modulus, 0.5×10^6 psi.
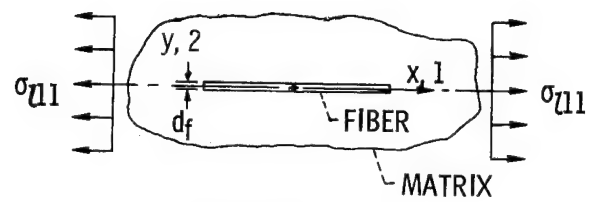
(a) Theoretical model.
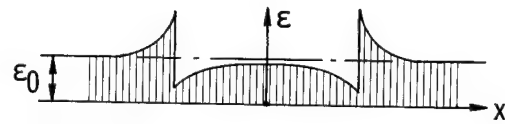
(b) Distribution of matrix strain along fiber.
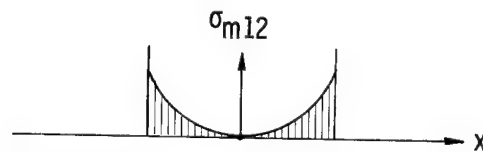
(c) Shear acting on matrix along joint line.

Figure 26. – Model analyzed by a finite element method. (From ref. 39.)
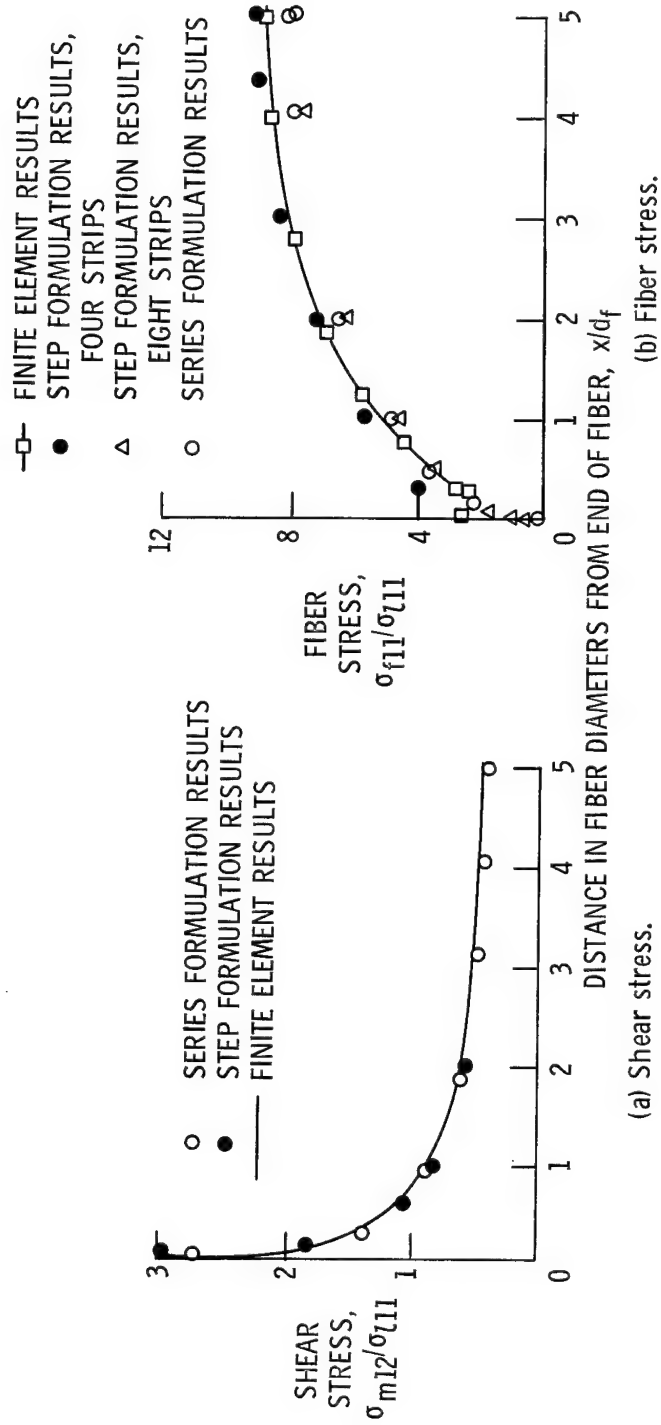
Figure 27. – Comparison of finite element results and other methods for axial tensile load. (From ref. 39.)
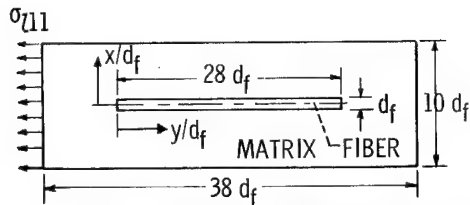
(a) Physical model of resin/glass composite with notation.
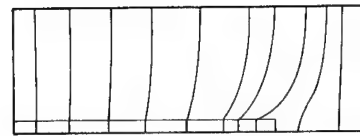
(b) Deformation mode for uniform applied load. Both fiber and matrix considered elastic.
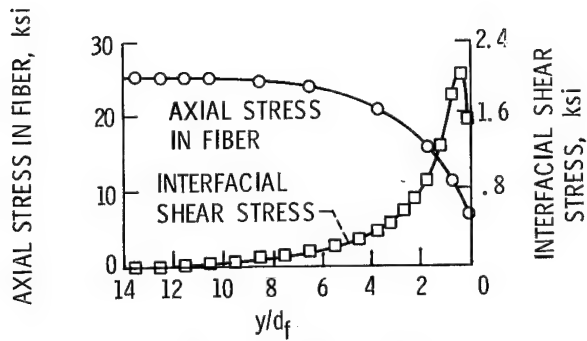
(c) Transfer of stress to fiber; a/b = 2.0; $\sigma_{\ell 11}$ = 1500 psi; E_f/E_m = 18.3.
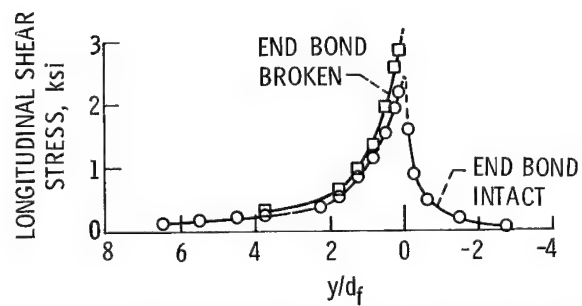
(d) Effect of end bond on interfacial shear stress a/b = 0.1; $\sigma_{\ell 11}$ = 1500 psi; E_f/E_m = 18.3.
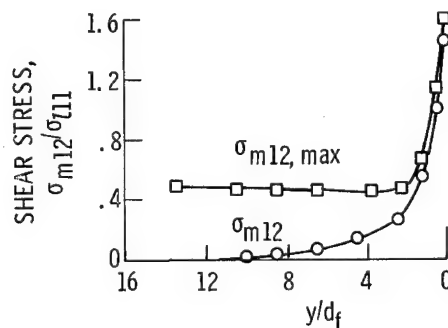
(e) Comparison of maximum shear with interfacial shear; a/b = 0.1; $\sigma_{\ell 11}$ = 1500 psi; E_f/E_m = 18.3.

Figure 28. – Finite element analysis model and results. (From ref. 35.)
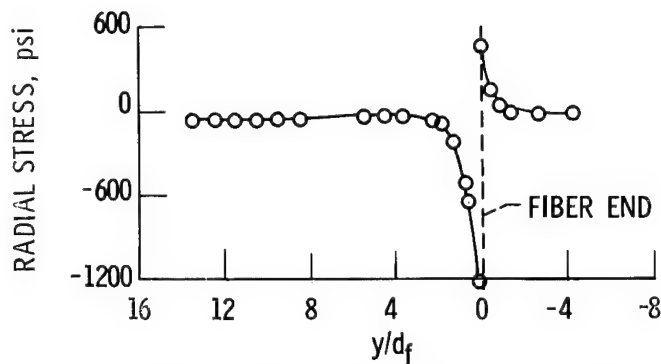
(a) Variation of radial stress along fiber; $a/b = 2.0$; $\sigma_{l11} = 1500$ psi; $x/d_f = 0.5$; $E_f/E_m = 18.3$.
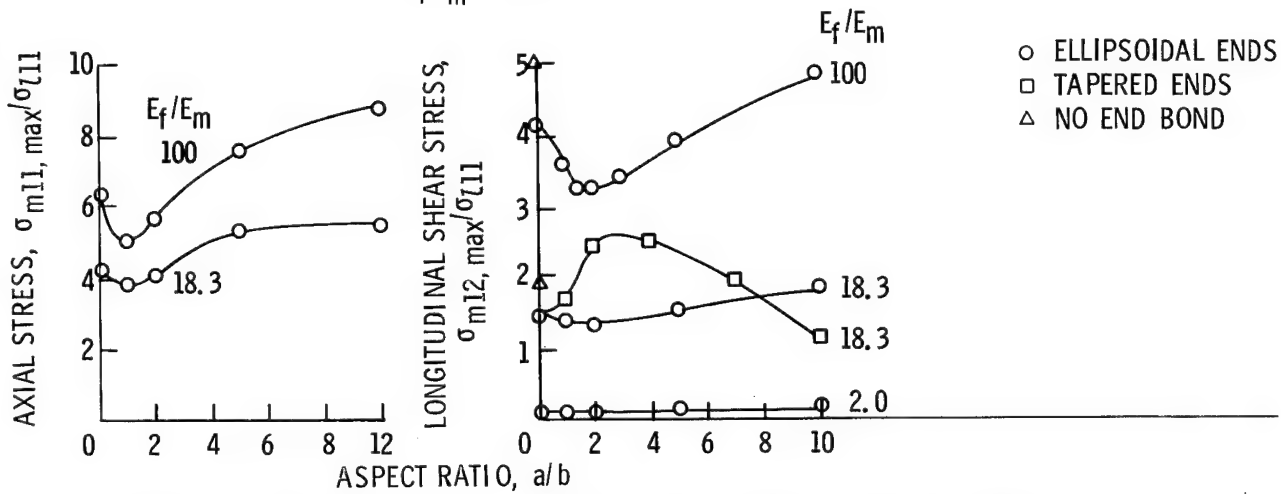
(b) Maximum matrix axial stress for different end geometries.

(c) Shear stress variation with end geometry.

Figure 29. – Finite element analysis results for different bonding, different end geometries, and different relative constituent fiber modulus ratios. (From ref. 35.)
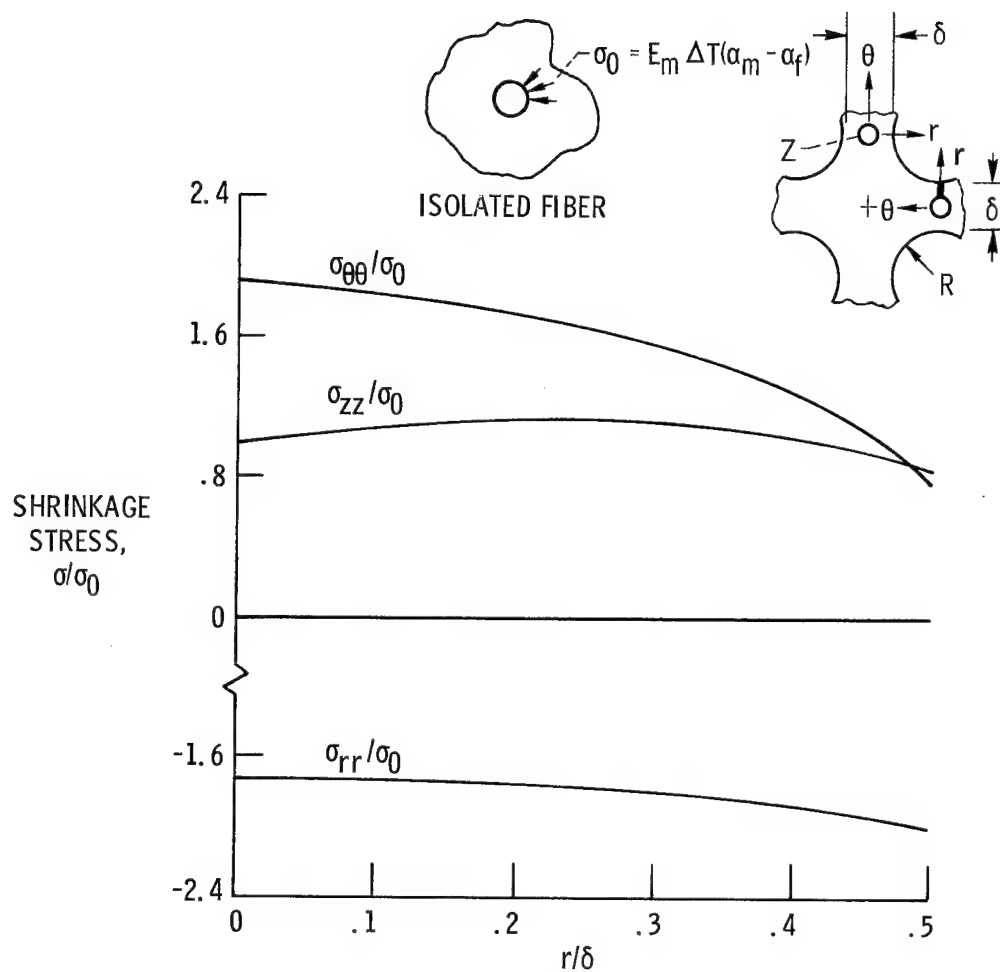
Figure 30. – Distribution of shrinkage stresses across section between fibers. Fiber volume ratio, ~0.5; $\delta/R = 0.5$. (From ref. 56.)
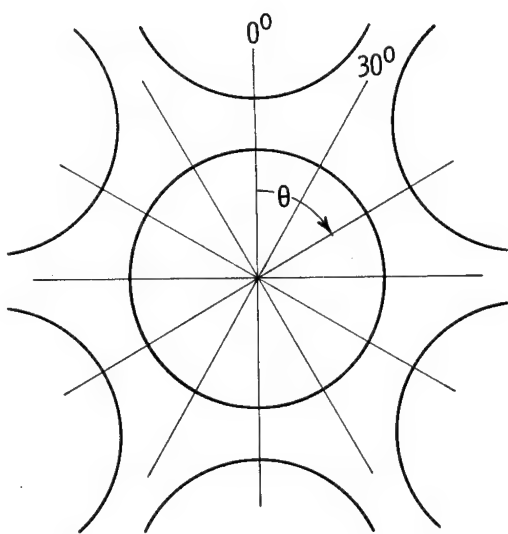
(a) Twelvefold symmetry lines in hexagonal array.
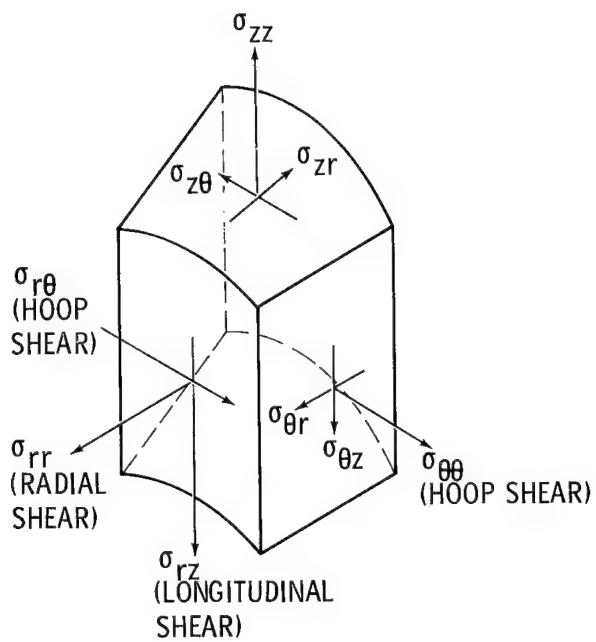
(b) Stresses on matrix element adjacent to fiber/matrix interface.

Figure 31. - General arrangement of a multifiber composite.

FIBER MODULUS, E_f, psi	MATRIX MODULUS, E_m, psi
60×10^6	0.38×10^6
10	0.38
10	1.00

(a) Radial stress.

(b) Resin hoop stress.

(c) Resin axial stress.

(d) Shear stress.

STRESS, ksi

ORIENTATION, θ, DEG
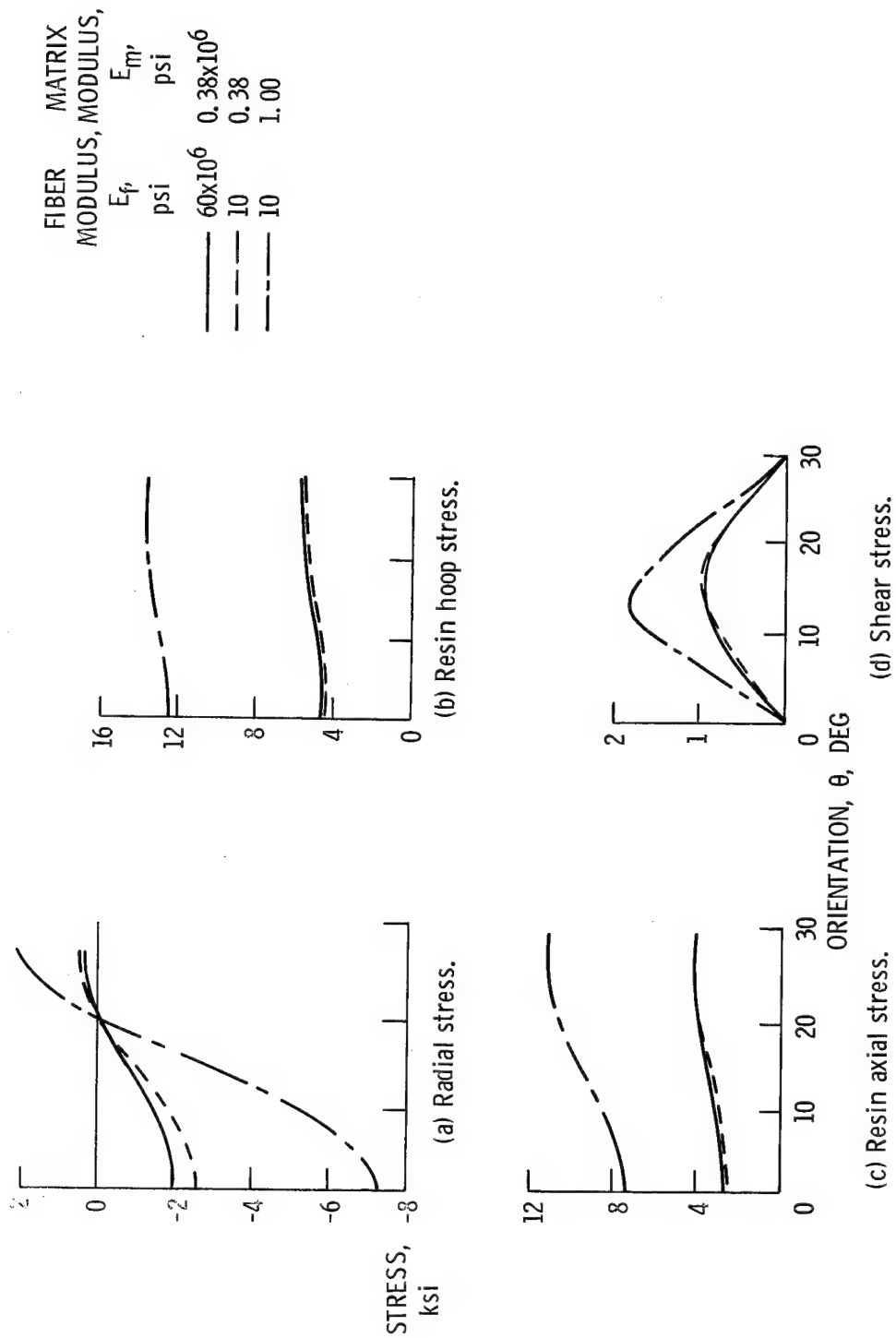
Figure 32. – Residual shrinkage stresses at interface for combinations of fiber and resin moduli at fiber volume ratio of 0.64 and $\alpha_m \Delta T \approx 0.01$. (From ref. 28.)

FIBER
VOLUME
RATIO

——— 0.64
- - - .70
-·— .80

STRESS,
ksi

(a) Radial stress.

ORIENTATION, θ, DEG

(b) Shear stress.

(c) Resin hoop stress.
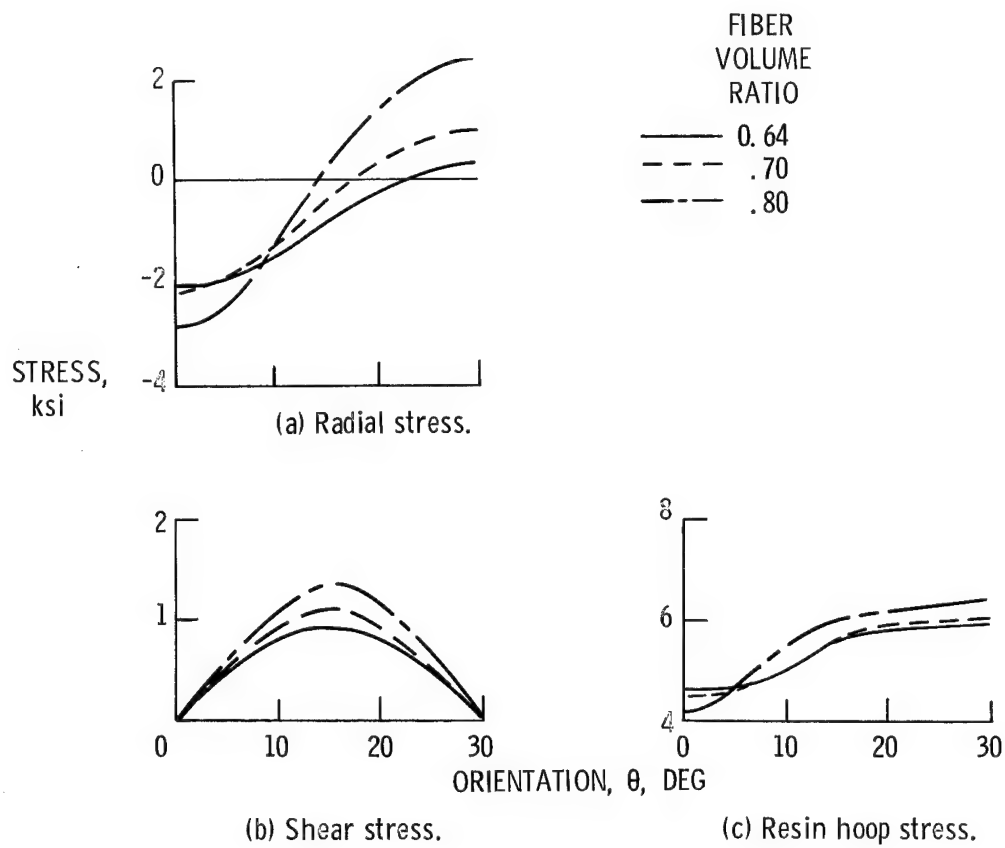
Figure 33. – Residual shrinkage stresses at interface for different fiber volume ratios. Fiber modulus, 60×10^6 psi; matrix modulus, 0.38×10^6 psi; $\alpha_m \, \Delta T$, ~0.01. (From ref. 28.)
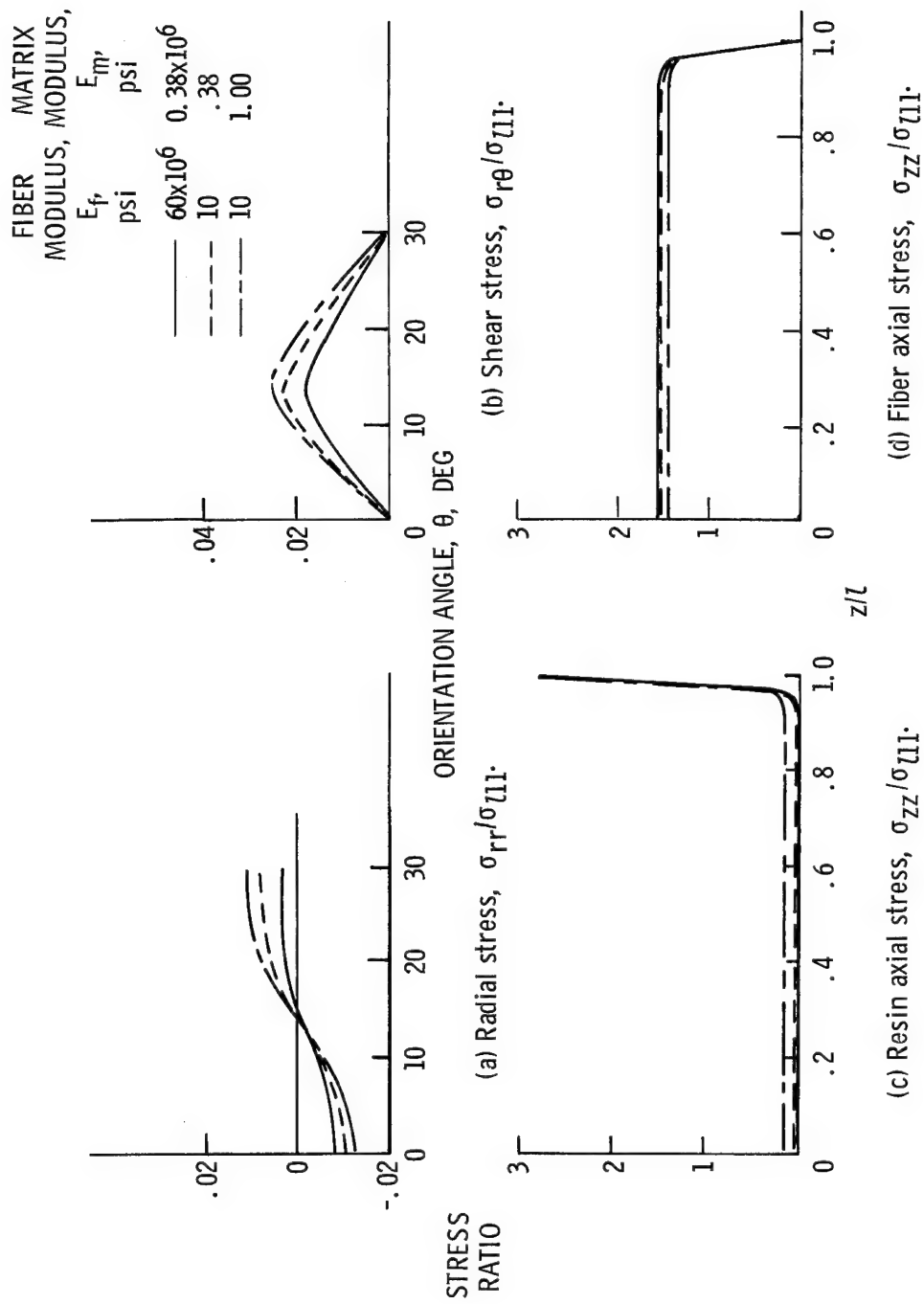
Figure 34. – Stresses at interface due to external load for combinations of fiber and resin moduli at fiber volume ratio of 0.64. (From ref. 28.)

FIBER VOLUME RATIO

——— 0.64
——— .70
—·—· .75
----- .80

(a) Radial stress, σ_{rr}/σ_{l11}.

STRESS RATIO

(b) Shear stress, $\sigma_{r\theta}/\sigma_{l11}$.

(c) Resin hoop stress, $\sigma_{\theta\theta}/\sigma_{l11}$.

ORIENTATION, θ, DEG
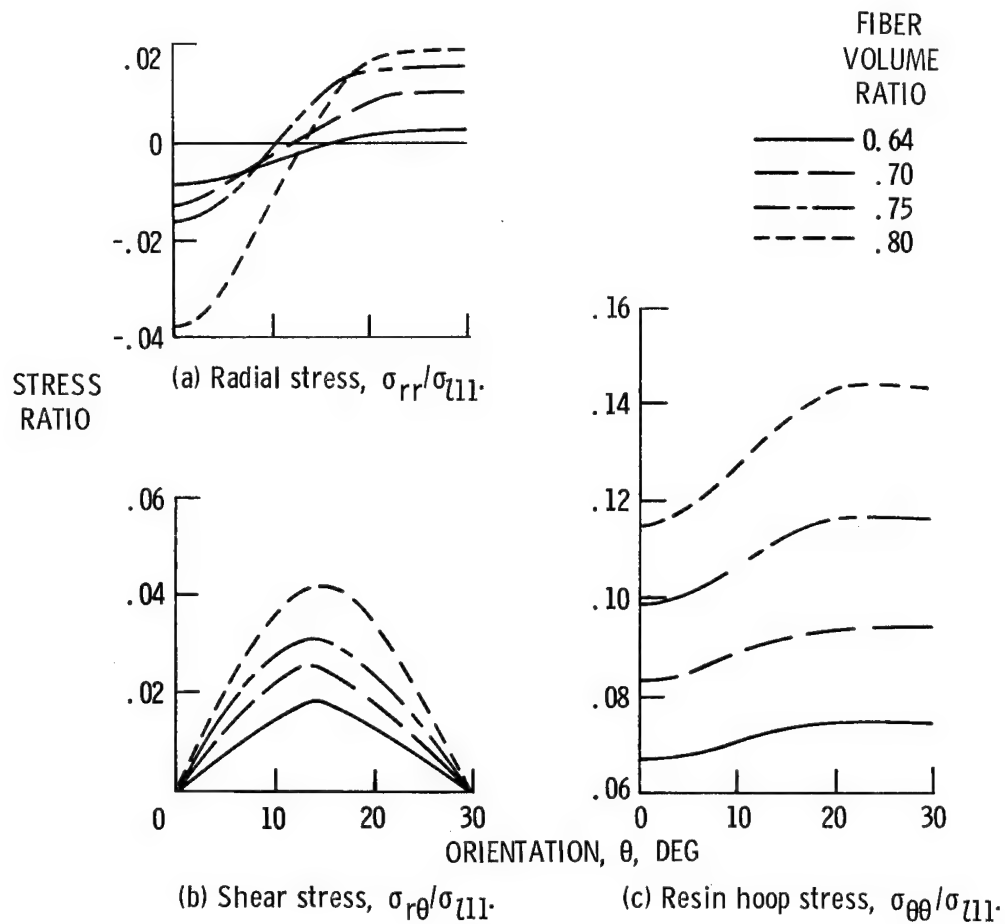
Figure 35. – Stresses at interface due to external load for different fiber volume ratios. Fiber modulus, 60×10^6 psi; matrix modulus, 0.38×10^6 psi. (From ref. 28.)

INEFFECTIVE FIBERS

VOIDS

FIBER

RESIN
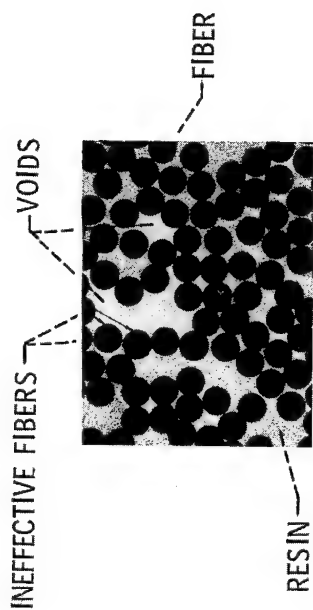
(a) Schematic of fiber-reinforced composite.

(b) Photomicrograph of actual composite.

(c) Volume ratio of ineffective fibers.

VOLUME RATIO
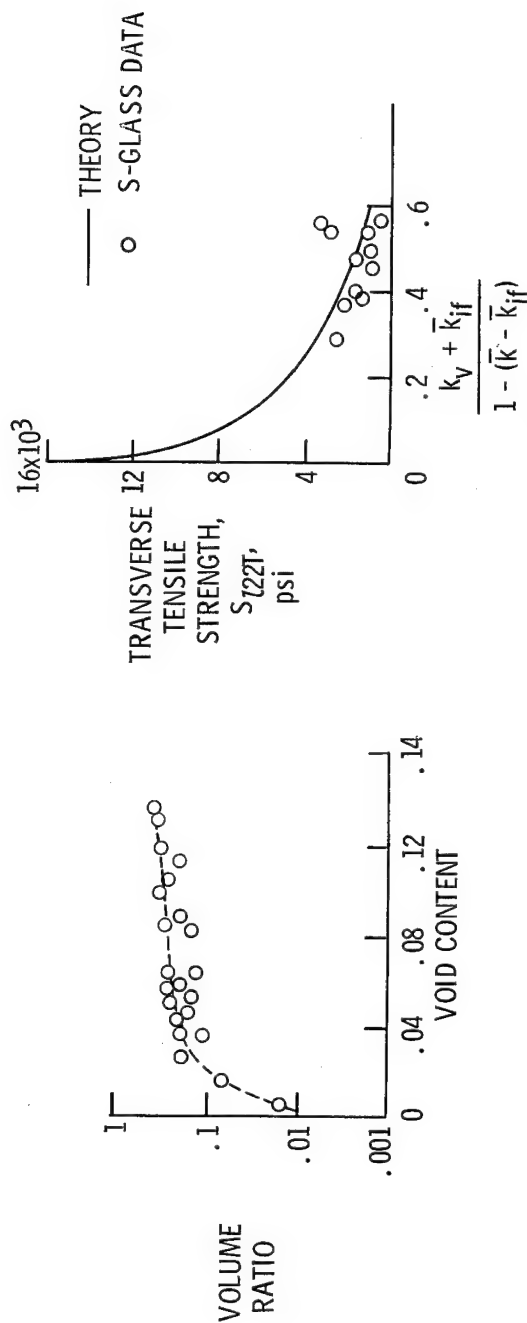
VOID CONTENT

(d) Test-theory comparison of micromechanics failure criteria.

TRANSVERSE TENSILE STRENGTH, S_{t22T}, psi

$$\frac{k_v + \bar{k}_{if}}{1 - (\bar{k} - \bar{k}_{if})}$$

—— THEORY
○ S-GLASS DATA

Figure 36. – Effect of voids on ineffective fiber content and transverse tensile strength of S-glass/epoxy composites. (From ref. 59.)

56

(a) Intralaminar shear strength. Fiber volume ratio, 0.56.

(b) Longitudinal compressive strength. Fiber volume ratio, 0.64.
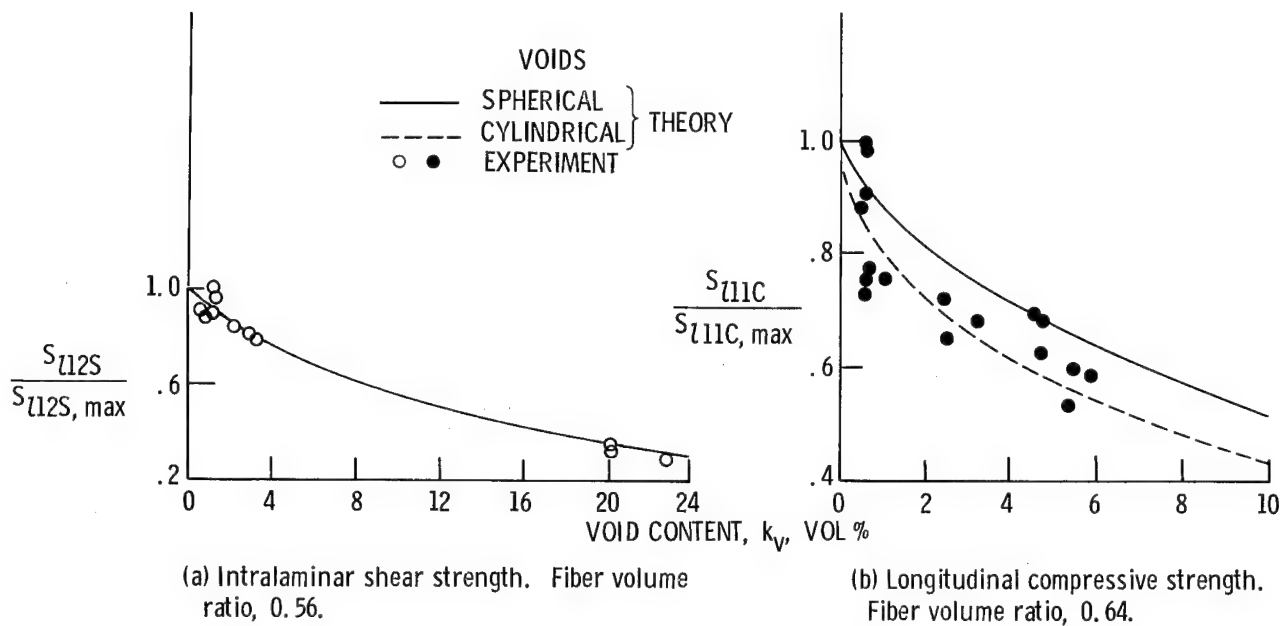
Figure 37. - Effect of voids on intralaminar and longitudinal compressive strengths for E-glass/epoxy composites. (From ref. 24.)
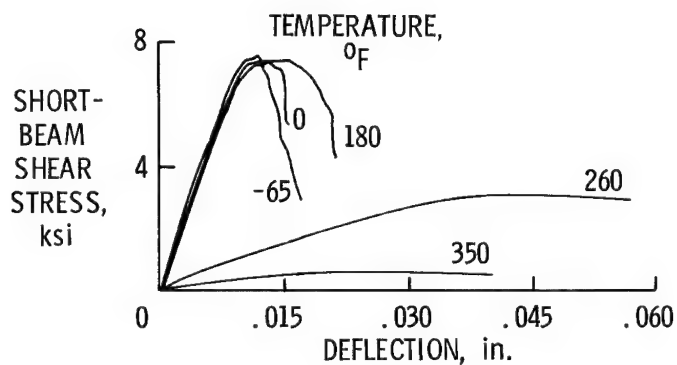
Figure 38. - Short-beam shear stress for graphite fiber/epoxy composites at various temperatures. Fiber modulus, 50×10^6 psi; fiber volume ratio, 0.5. (From ref. 60.)

ENVIRONMENT

——— 21° C, SEA WATER
——— 74° C, 25% RELATIVE HUMIDITY
—·—· 74° C, 100% RELATIVE HUMIDITY
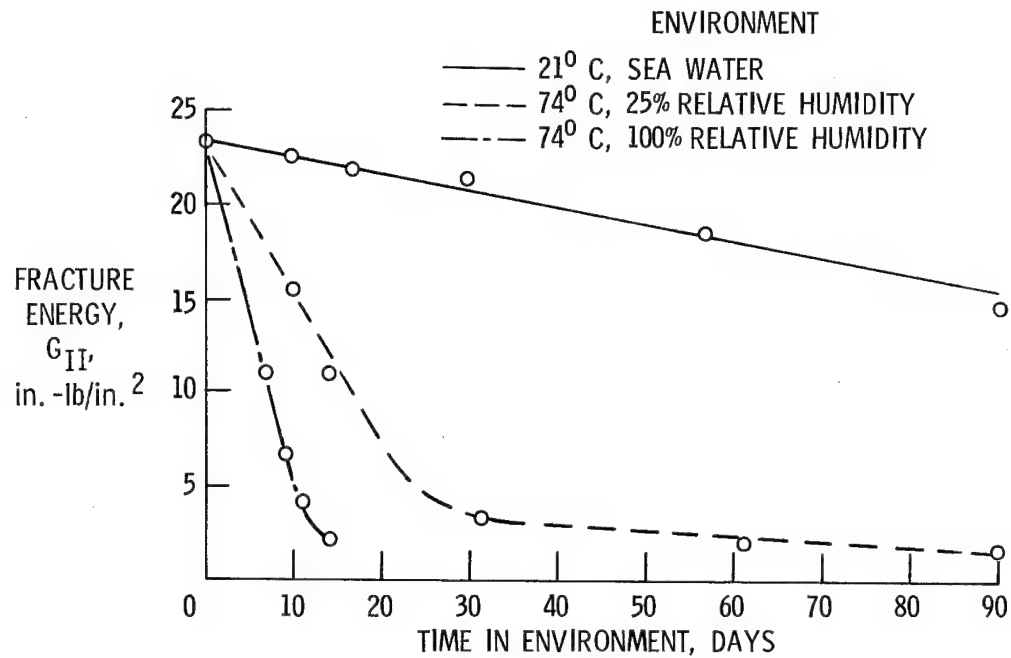
Figure 39. – Effect of time in various environments on debonding fracture energy between glass and resin. (From ref. 45.)
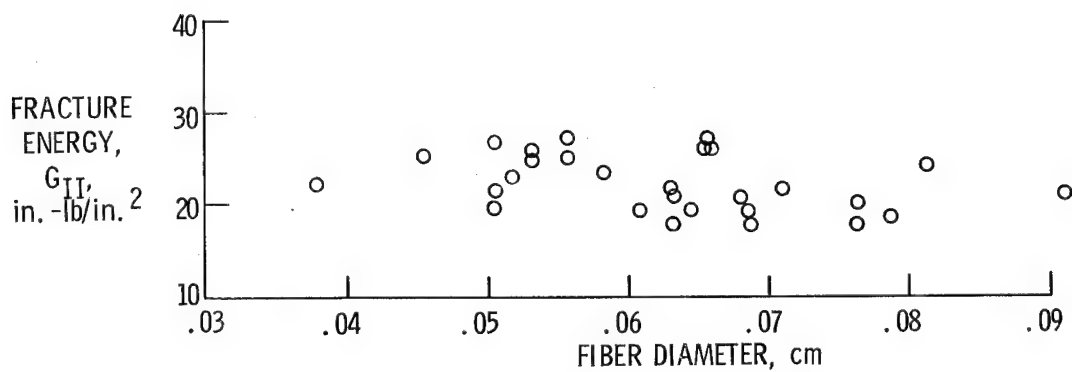
Figure 40. – Debonding fracture energy as function of fiber diameter. (From ref. 45.)

58
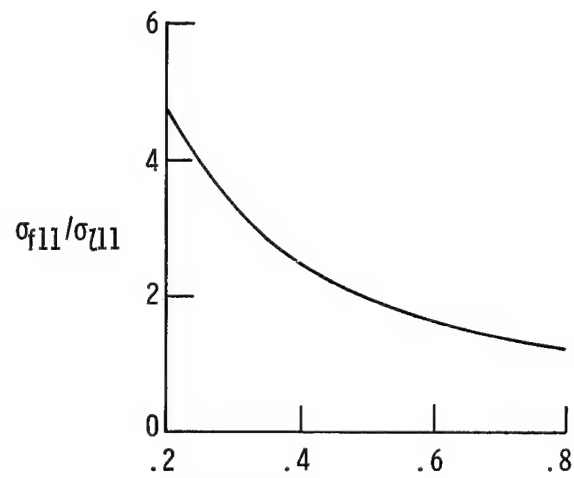
(a) Fiber effective applied stress.
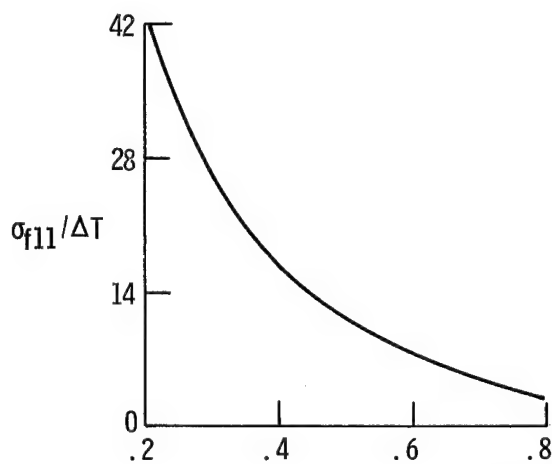
(b) Fiber effective thermal stress.
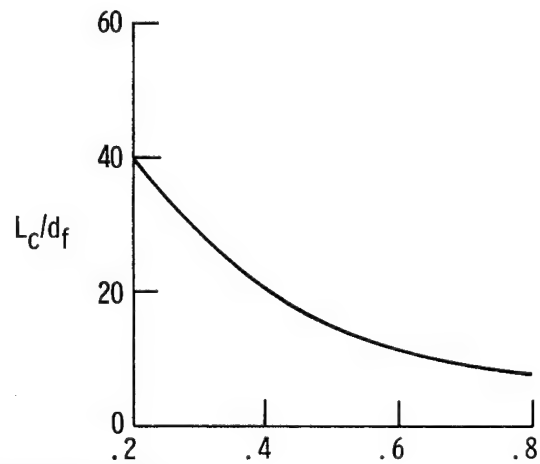
(c) Fiber ineffective length.

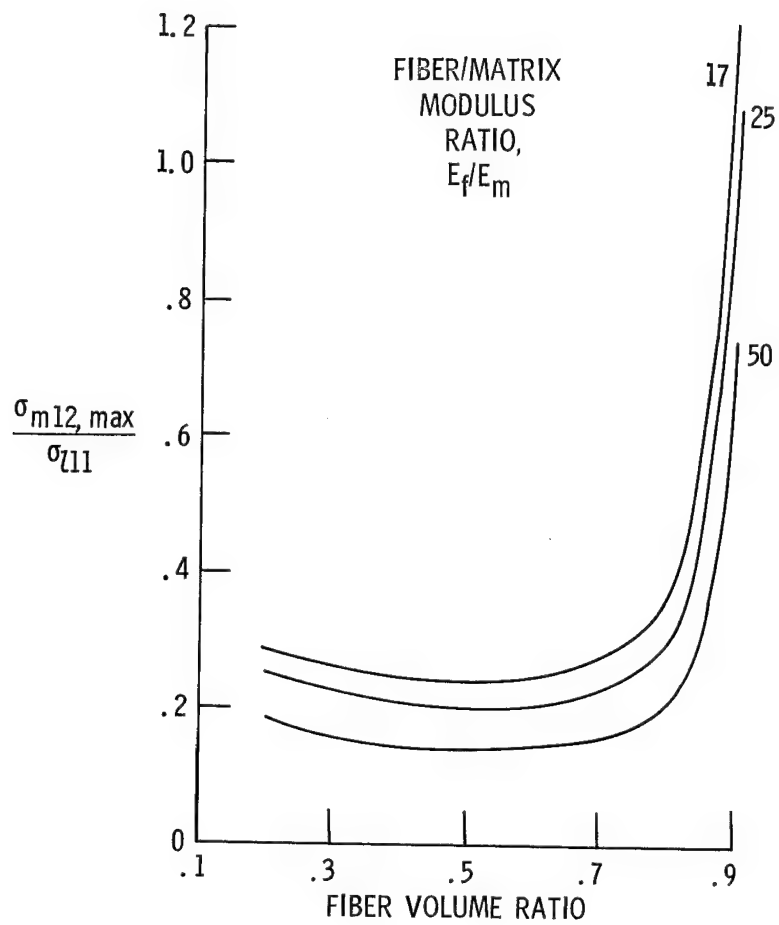Figure 41. – Interfacial bond influence on load transfer in unidirectional S-glass composites.

Figure 42. – Theoretical interfacial bond
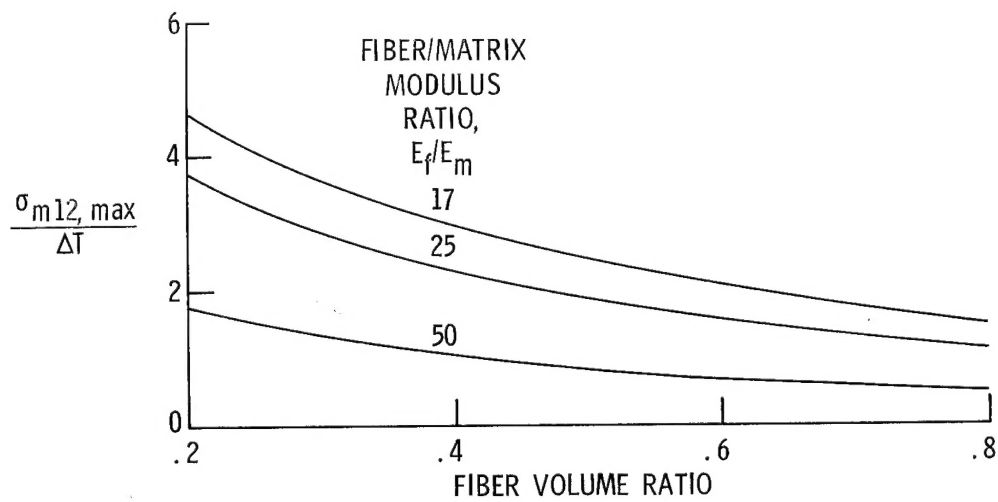maximum shear concentration for
S-glass/epoxy composites.

Figure 43. - Maximum shear stress concentration at interface due to thermal load.
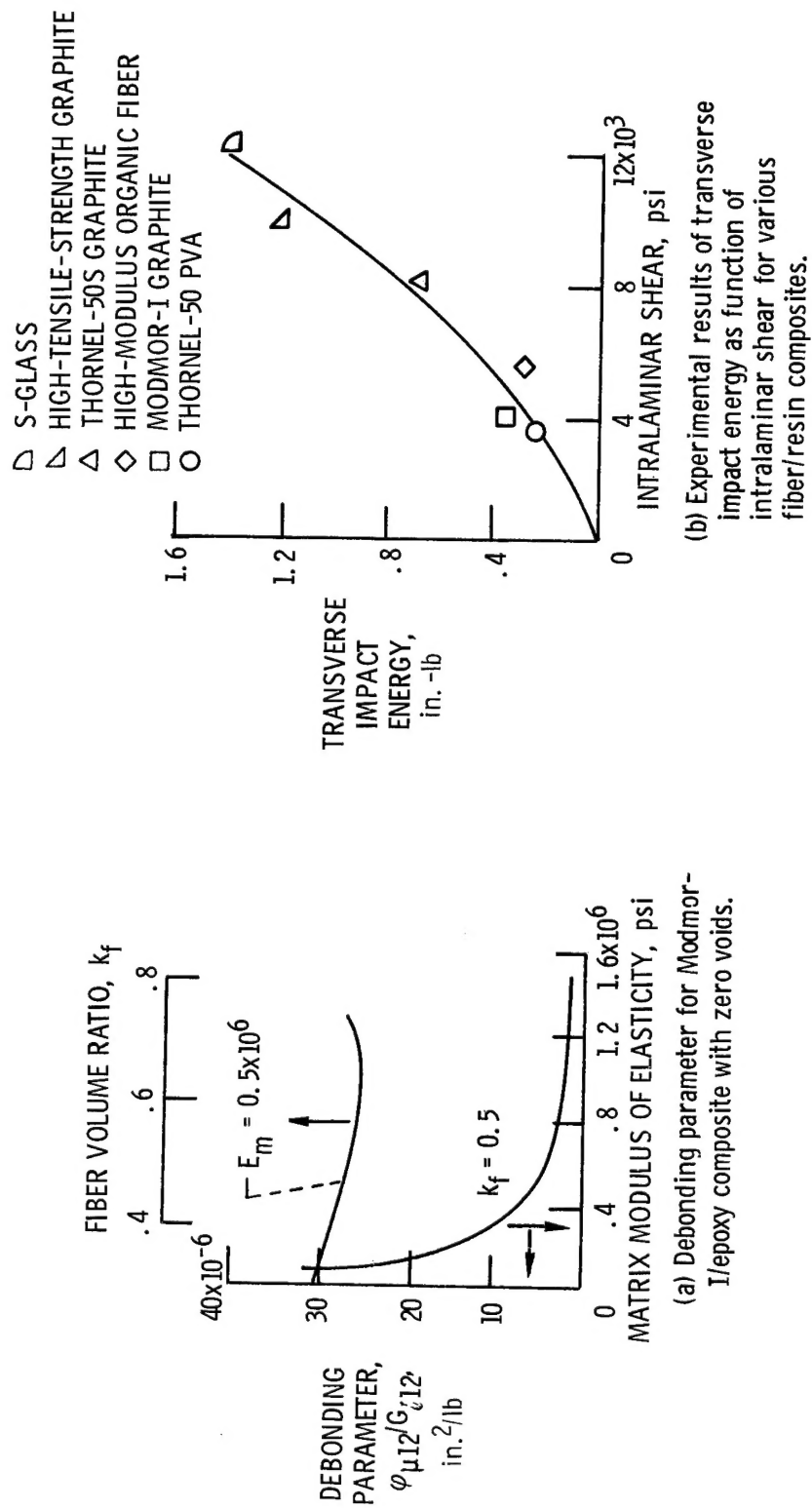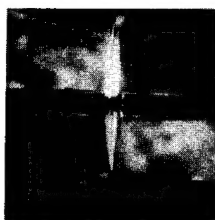
DEBONDING
PARAMETER,
$\varphi_{\mu 12}/G_{\iota 12}$,
in.^{2}/lb

FIBER VOLUME RATIO, k_f

$E_m = 0.5 \times 10^6$

$k_f = 0.5$

MATRIX MODULUS OF ELASTICITY, psi

(a) Debonding parameter for Modmor-I/epoxy composite with zero voids.

△ S-GLASS
△ HIGH-TENSILE-STRENGTH GRAPHITE
△ THORNEL-50S GRAPHITE
◇ HIGH-MODULUS ORGANIC FIBER
◇ MODMOR-I GRAPHITE
□ MODMOR-I GRAPHITE
○ THORNEL-50 PVA

TRANSVERSE
IMPACT
ENERGY,
in.-lb

INTRALAMINAR SHEAR, psi

(b) Experimental results of transverse impact energy as function of intralaminar shear for various fiber/resin composites.

Figure 44. – Parameters and relations useful in selecting constituents for specified interface conditions. (From ref. 54.)
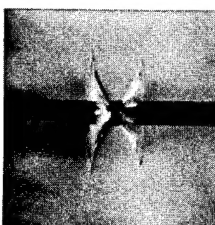
62

(a) High-energy radial crack normal to fiber.

(b) Interface unbonding due to high shear stress at newly formed ends.
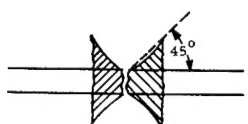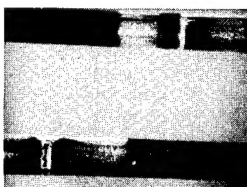
(c) Low-energy resolved-shear-stress-induced tensile cracks in matrix.

CS-59177

Figure 45. – Failure mechanisms in boron/epoxy. (From ref. 52.)

"The aeronautical and space activities of the United States shall be conducted so as to contribute . . . to the expansion of human knowledge of phenomena in the atmosphere and space. The Administration shall provide for the widest practicable and appropriate dissemination of information concerning its activities and the results thereof."

— NATIONAL AERONAUTICS AND SPACE ACT OF 1958

NASA SCIENTIFIC AND TECHNICAL PUBLICATIONS

TECHNICAL REPORTS: Scientific and technical information considered important, complete, and a lasting contribution to existing knowledge.

TECHNICAL NOTES: Information less broad in scope but nevertheless of importance as a contribution to existing knowledge.

TECHNICAL MEMORANDUMS: Information receiving limited distribution because of preliminary data, security classification, or other reasons.

CONTRACTOR REPORTS: Scientific and technical information generated under a NASA contract or grant and considered an important contribution to existing knowledge.

TECHNICAL TRANSLATIONS: Information published in a foreign language considered to merit NASA distribution in English.

SPECIAL PUBLICATIONS: Information derived from or of value to NASA activities. Publications include conference proceedings, monographs, data compilations, handbooks, sourcebooks, and special bibliographies.

TECHNOLOGY UTILIZATION PUBLICATIONS: Information on technology used by NASA that may be of particular interest in commercial and other non-aerospace applications. Publications include Tech Briefs, Technology Utilization Reports and Technology Surveys.

Details on the availability of these publications may be obtained from:

SCIENTIFIC AND TECHNICAL INFORMATION OFFICE

NATIONAL AERONAUTICS AND SPACE ADMINISTRATION
Washington, D.C. 20546